Cellular/Molecular

HDAC2 in Primary Sensory Neurons Constitutively Restrains Chronic Pain by Repressing α2δ-1 Expression and Associated NMDA Receptor Activity

Jixiang Zhang (张吉祥),[1*] Shao-Rui Chen (陈少瑞),[1*] Meng-Hua Zhou (周孟华),[1] Daozhong Jin (金道忠),[1] Hong Chen (陈红),[1] Li Wang (王力),[1] Ronald A. DePinho,[2] and Hui-Lin Pan (潘惠麟)[1]

[1]Center for Neuroscience and Pain Research, Department of Anesthesiology and Perioperative Medicine, University of Texas MD Anderson Cancer Center, Houston, Texas 77030, and [2]Department of Cancer Biology, University of Texas MD Anderson Cancer Center, Houston, Texas 77030

α2δ-1 (encoded by the *Cacna2d1* gene) is a newly discovered NMDA receptor-interacting protein and is the therapeutic target of gabapentinoids (e.g., gabapentin and pregabalin) frequently used for treating patients with neuropathic pain. Nerve injury causes sustained α2δ-1 upregulation in the dorsal root ganglion (DRG), which promotes NMDA receptor synaptic trafficking and activation in the spinal dorsal horn, a hallmark of chronic neuropathic pain. However, little is known about how nerve injury initiates and maintains the high expression level of α2δ-1 to sustain chronic pain. Here, we show that nerve injury caused histone hyperacetylation and diminished enrichment of histone deacetylase-2 (HDAC2), but not HDAC3, at the *Cacna2d1* promoter in the DRG. Strikingly, *Hdac2* knockdown or conditional knockout in DRG neurons in male and female mice consistently induced long-lasting mechanical pain hypersensitivity, which was readily reversed by blocking NMDA receptors, inhibiting α2δ-1 with gabapentin or disrupting the α2δ-1–NMDA receptor interaction at the spinal cord level. *Hdac2* deletion in DRG neurons increased histone acetylation levels at the *Cacna2d1* promoter, upregulated α2δ-1 in the DRG, and potentiated α2δ-1–dependent NMDA receptor activity at primary afferent central terminals in the spinal dorsal horn. Correspondingly, *Hdac2* knockdown-induced pain hypersensitivity was blunted in *Cacna2d1* knockout mice. Thus, our findings reveal that HDAC2 functions as a pivotal transcriptional repressor of neuropathic pain via constitutively suppressing α2δ-1 expression and ensuing presynaptic NMDA receptor activity in the spinal cord. HDAC2 enrichment levels at the *Cacna2d1* promoter in DRG neurons constitute a unique epigenetic mechanism that governs acute-to-chronic pain transition.

Key words: **chromatin; dorsal root ganglion; epigenetics; histone modification; synaptic plasticity; transcriptomics**

Significance Statement

Excess α2δ-1 proteins produced after nerve injury directly interact with glutamate NMDA receptors to potentiate synaptic NMDA receptor activity in the spinal cord, a prominent mechanism of nerve pain. Because α2δ-1 upregulation after nerve injury is long lasting, gabapentinoids relieve pain symptoms only temporarily. Our study demonstrates for the first time the unexpected role of intrinsic HDAC2 activity at the α2δ-1 gene promoter in limiting α2δ-1 gene transcription, NMDA receptor-dependent synaptic plasticity, and chronic pain development after nerve injury. These findings challenge the prevailing view about the role of general HDAC activity in promoting chronic pain. Restoring the repressive HDAC2 function and/or reducing histone acetylation at the α2δ-1 gene promoter in primary sensory neurons could lead to long-lasting relief of nerve pain.

Received Apr. 13, 2022; revised Oct. 3, 2022; accepted Oct. 10, 2022.

Author contributions: H.-L.P. designed research; J.Z., S.-R.C., M.-H.Z., D.J., H.C., and L.W. performed research; R.A.D. contributed unpublished reagents/analytic tools; J.Z., S.-R.C., M.-H.Z., D.J., H.C., L.W., and H.-L.P. analyzed data; J.Z., S.-R.C., and H.-L.P. wrote the paper.

This work was supported by National Institutes of Health–National Institute of Neurological Disorders and Stroke Grant NS101880 and the N.G. and Helen T. Hawkins Endowment. We thank Sarah Bronson at MD Anderson Cancer Center for proofreading the manuscript.

*J.Z. and S.-R.C. contributed equally to this work.

The authors are employees of the University of Texas System, which currently holds a patent for targeting α2δ-1–bound glutamate receptors for treating diseases and disorders.

Correspondence should be addressed to Hui-Lin Pan at huilinpan@mdanderson.org.

https://doi.org/10.1523/JNEUROSCI.0735-22.2022

Introduction

Neuropathic pain is a chronic debilitating condition that afflicts millions of people worldwide. Current treatments are unsatisfactory, and our knowledge of the underlying mechanisms governing neuropathic pain development remains limited. Both sustained changes in gene expression in primary sensory neurons and synaptic plasticity in the spinal dorsal horn are integral to the development of chronic neuropathic pain (Woolf and Salter, 2000; Zhou et al., 2011; Laumet et al., 2015). Among many upregulated genes in the dorsal root ganglion (DRG) caused by nerve injury, α2δ-1 (encoded by the *Cacna2d1* gene)

Table 1. List of primers used in this study

Primer name	Sequence 5′–3′	Experiment
*Hdac2*_P14F	ATT TGG GAG AAG GCC AGT TT	Genotyping *Hdac2*-flox
Hdac2 P15R	AAT TTC ACA GCC CCA GCT AAG	Genotyping *Hdac2*-flox
*Hdac2*_P2	CGA AAT ACC TGG GTA GAT AAA GC	Genotyping *Hdac2*-flox
Avl-Cre-1	CCC TGT TCA CTG TGA GTA GG	Genotyping *Avl*-Cre
Avl-Cre-2	AGT ATC TGG TAG GTG CTT CCA G	Genotyping *Avl*-Cre
Avl-Cre-3	GCG ATC CCT GAA CAT GTC CAT C	Genotyping *Avl*-Cre
Avl-icre-transgene forward	ACC CCG ACT TTG TGA TGT TTC	Genotyping *Avl*-Cre^{ERT2}
Avl-icre-transgene reverse	CTG CCT GTC CCT GAA CAT G	Genotyping *Avl*-Cre^{ERT2}
Avl-icre-internal positive control forward	CAC GTG GGC TCC AGC ATT	Genotyping *Avl*-Cre^{ERT2}
Avil-icre-internal positive control reverse	TCA CCA GTC ATT TCT GCC TTT G	Genotyping *Avl*-Cre^{ERT2}
Cacna2d1-Primer A	CAT GGG TGG ACA AGA TGC AAG	Genotyping *Cacna2d1* KO
Cacna2d1-Primer B	CTG CAC GAG ACT AGT GAG ACG	Genotyping *Cacna2d1* KO
Cacna2d1-Primer C	CAT TCT CAA GAC TGT AGG CAG AG	Genotyping *Cacna2d1* KO
Rat *Hdac3* forward	CCC CAG ATT TCA CGC TCC AT	RT-PCR
Rat *Hdac3* reverse	TGA ATC TGG ACA CTG GGT G	RT-PCR
Rat *Cacna2d1* forward	GGA CCT ATT CAG TGG ATG GCT TG	RT-PCR
Rat *Cacna2d1* reverse	CCA TTG GTC TTC CCA GAA CAT CTA GA	RT-PCR
Rat *Hdac2* forward	GAT GAG GAT GGA GAA GAC CCT G	RT-PCR
Rat *Hdac2* reverse	ATG ATC AGC GAC ATT CCT ACG ACC	RT-PCR
Rat *Gapdh* forward	CAT CCC AGA GCT GAA CGG GAA G	RT-PCR
Rat *Gapdh* reverse	GTC CTC AGT GTA GCC CAG GAT GC	RT-PCR
Mouse *Hdac2* forward	GCT GGA GGA CTA CAT CAT GCC A	RT-PCR
Mouse *Hdac2* reverse	ACC ATC ACC ATG GTG GAT GTC TAT G	RT-PCR
Mouse *Cacna2d1* forward	GGG TGG ACA AGA TGC AAG AAG AC	RT-PCR
Mouse *Cacna2d1* reverse	TGG CGT GCA TTG TTG GGC TC	RT-PCR
Mouse *Tuba1a* forward	CCA CTA CAC CAT TGG CAA GGA GA	RT-PCR
Mouse *Tuba1a* reverse	GGA GGT GAA GCC AGA GCC AGT	RT-PCR
Mouse *Cacna2d1* ChIP promoter forward	CTG GCC GAG CTC TGT TTC CAC AGT	ChIP-PCR (71 to 164 bp)
Mouse *Cacna2d1* ChIP promoter reverse	GGG CGG ACT CTC TAG CGC GTG GCT	ChIP-PCR
Mouse *Cacna2d1* ChIP UTR forward	GAC ATG GGA CTA ACG TAC TAT GCA AAG	ChIP-PCR (440,221 to 440,390 bp)
Mouse *Cacna2d1* ChIP UTR reverse	TGC TCT ACT TCA TGC AAT ACT TCA GTG C	ChIP-PCR
Mouse *Gapdh* ChIP promoter forward	TCT CAG GTT CCG AGG AGG GAT AC	ChIP-PCR (−53 to 85 bp)
Mouse *Gapdh* ChIP promoter reverse	TTG AGA CTT ACA AAC ACT CTC CTG AG	ChIP-PCR
Rat *Cacna2d1* ChIP promoter forward	CCT CTC CTC GGC GAC CGC AGA TAA A	ChIP-PCR (−32 to 60 bp)
Rat *Cacna2d1* ChIP promoter reverse	ACT GTG GAA ACG GAG CTC GGC CAG	ChIP-PCR
Rat *Gapdh* ChIP forward	CAT TGC AGA GGA TGG TAG AGG A	ChIP-PCR (−120 to −23 bp)
Rat *Gapdh* ChIP reverse	GGA GAA GAA AGT CAG ATT AGC GTG G	ChIP-PCR

Table 2. List of antibodies used in this study

Antibody	Source	Experiment
Rabbit anti-HDAC2	Catalog #ab7029, Abcam	Immunoblotting (1:5000 dilution)
Rabbit anti-$\alpha 2\delta$-1	Catalog #ACC-015, Alomone Labs	Immunoblotting (1:500)
Rabbit anti-GAPDH	Catalog #5174, Cell Signaling Technology	Immunoblotting (1:5000 dilution)
Mouse anti-β-actin	Catalog #3700, Cell Signaling Technology	Immunoblotting (1:2000 dilution)
Mouse anti-PSD-95	Catalog #75–028, NeuroMab	Immunoblotting (1:2000 dilution)
HRP-conjugated anti-rabbit IgG (secondary)	Catalog #111–035-144, Jackson ImmunoResearch	Immunoblotting (1:10 000 dilution)
HRP-conjugated anti-mouse IgG (secondary)	Catalog #7076, Cell Signaling Technology	Immunoblotting (1:10 000 dilution)
Rabbit anti-HDAC2	Catalog #ab7029, Abcam	Immunocytochemistry (1:500 dilution)
Mouse anti-NeuN	Catalog #ab104224, Abcam	Immunocytochemistry (1:200 dilution)
Rabbit IgG isotype control	Catalog #2729, Cell Signaling Technology	ChIP
Rabbit anti-HDAC2	Catalog #ab7029, Abcam	ChIP
Rabbit anti-HDAC3	Catalog #ab7030, Abcam	ChIP
Rabbit anti-H3	Catalog #2650, Cell Signaling Technology	ChIP
Rabbit anti-H3ac	Catalog #06–599, Millipore	ChIP
Rabbit anti-H4ac	Catalog #06–866, Millipore	ChIP
Rabbit anti-H4K5ac	Catalog #07–327, Millipore	ChIP
Rabbit anti-H3K9ac	Catalog #9649, Cell Signaling Technology	ChIP
Rabbit anti-H3K14ac	Catalog #7627, Cell Signaling Technology	ChIP

is the best known and clinically validated target in the treatment of neuropathic pain (Gee et al., 1996; Fuller-Bicer et al., 2009). $\alpha 2\delta$-1 mediates the therapeutic effect of gabapentinoids, including gabapentin and pregabalin, which are first-line drugs for treating neuropathic pain. Peripheral nerve injury induces an early and sustained increase in $\alpha 2\delta$-1 expression in DRG neurons (Luo et al., 2001; Newton et al., 2001; Zhang et al., 2021). Another hallmark of neuropathic pain is increased

glutamatergic input augmented by NMDAR receptor hyperactivity in the spinal dorsal horn (Zhang et al., 2009; Zhou et al., 2012; Chen et al., 2014b; Li et al., 2016; Xie et al., 2017). Previous studies revealed that in neuropathic pain, excess $\alpha2\delta$-1 proteins physically interact with NMDARs to potentiate NMDAR synaptic trafficking and activity in the spinal dorsal horn independently of voltage-gated Ca^{2+} channels (Chen et al., 2018, 2019; Zhang et al., 2021). However, little is known about how nerve injury initiates and maintains the high expression level of $\alpha2\delta$-1 and associated NMDAR activity to sustain chronic pain.

Chromatin structure and the modification status of histone tails critically control gene transcription (Strahl and Allis, 2000; Jiang et al., 2008), and altered expression levels of pronociceptive and antinociceptive genes in the DRG are causally related to the development of chronic pain after nerve injury. For example, G9a, a histone methyltransferase, facilitates chronic pain development after nerve injury by silencing antinociceptive genes, including genes associated with 40 voltage-gated K^+ channels and μ-opioid and cannabinoid receptors (Laumet et al., 2015; Zhang et al., 2016; Luo et al., 2020). Also, nerve injury induces sustained DNA hypomethylation of many genes in the DRG (Garriga et al., 2018). However, altering histone methylation or DNA methylation does not normalize $\alpha2\delta$-1 expression levels in the injured DRG (Laumet et al., 2015; Garriga et al., 2018). Acetylation is another common modification of histones and serves as a crucial epigenetic mechanism for gene transcription. The acetylation status of lysine residues in histone tails is dynamically regulated by the opposing activities of various histone acetyltransferases and histone deacetylases (HDACs). HDAC proteins are grouped into four classes based on function and DNA sequence similarity, and Class I HDAC subtypes (HDAC1, HDAC2, HDAC3, and HDAC8) are located primarily in the nucleus. The functions of Class I HDACs in the nervous system are highly heterogeneous. In the brain, HDAC1 is predominantly expressed in glia, whereas HDAC2 is abundant in mature neurons and is involved in memory formation (Broide et al., 2007; Guan et al., 2009; Hanson et al., 2013). At present, the roles of individual HDAC subtypes in regulating the transcription of *Cacna2d1* and the development of neuropathic pain remain unclear.

Here, we present our findings that nerve injury diminishes HDAC2 occupancy at the promoter region of *Cacna2d1* in the DRG, which induces histone hyperacetylation and promotes the transcription of *Cacna2d1*. Strikingly, knockdown or conditional knockout (KO) of *Hdac2* in DRG neurons causes a neuropathic pain-like phenotype, which is maintained by $\alpha2\delta$-1–dependent NMDAR activation in the spinal dorsal horn. Thus, our study uncovers HDAC2 as a crucial epigenetic repressor of chronic pain development via constitutive suppression of *Cacna2d1* transcription in primary sensory neurons and associated synaptic NMDAR activity in the spinal cord. This information advances our understanding of the epigenetic basis of chronic neuropathic pain.

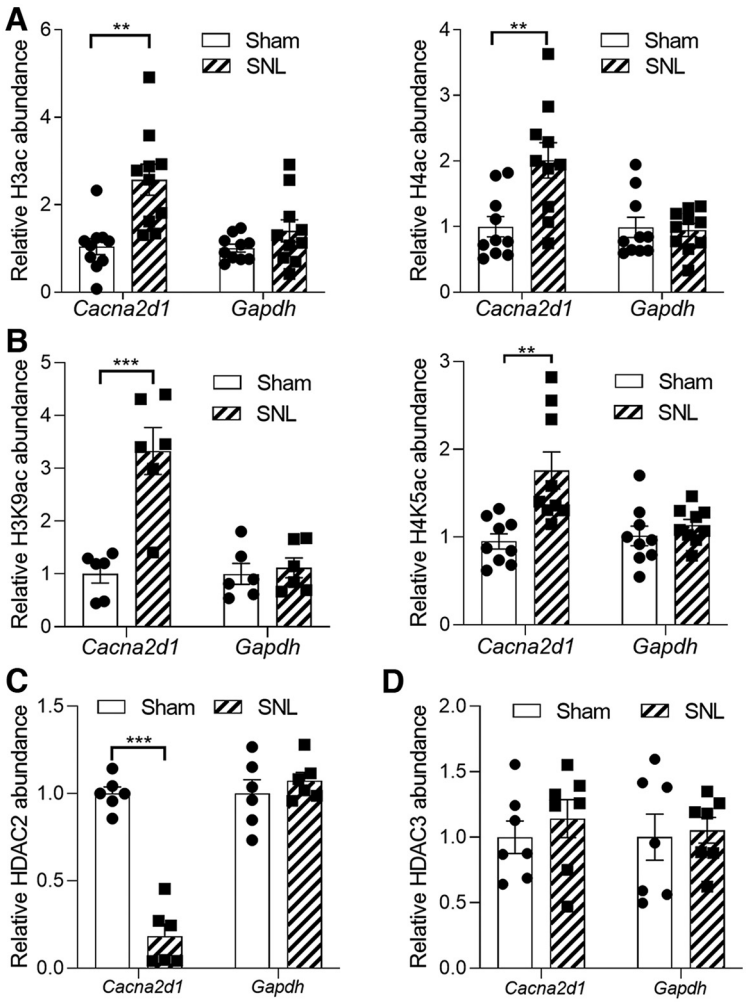

Figure 1. Nerve injury diminishes HDAC2 occupancy and causes histone hyperacetylation at the *Cacna2d1* promoter in the DRG. ***A***, Total H3ac and H4ac levels at the promoters of *Cacna2d1* (−32 to 60 bp) and *Gapdh* (−120 to −23 bp) in the DRG from rats subjected to sham surgery or SNL; $^{**}p < 0.01$, two-tailed *t* test, $n = 10$ rats per group. ***B***, H3K9ac and H4K5ac levels at the promoters of *Cacna2d1* and *Gapdh* in the DRG from rats subjected to sham surgery or SNL; $^{**}p < 0.01$, $^{***}p < 0.001$, two-tailed *t* test, $n = 6$ rats per group for H3K9ac, $n = 9$ rats for H4K5ac. ***C***, ***D***, The occupancy of HDAC2 (***C***) and HDAC3 (***D***) at the promoters of *Cacna2d1* and *Gapdh* in the DRG from rats subjected to sham surgery or SNL; $^{***}p < 0.001$, two-tailed *t* test, $n = 6$ rats per group for HDAC2, $n = 7$ rats per group for HDAC3. Data are expressed as means ± SEM.

Materials and Methods

Animal models. All procedures and experimental protocols were approved by the Institutional Animal Care and Use Committee at The University of Texas MD Anderson Cancer Center and conformed to guidelines from the National Institutes of Health on the ethical use of animals. All animals were housed (two to three per cage for rats, and four to five per cage for mice) on a standard 12 h light/dark cycle, maintained in pathogen-free conditions, and received food and water *ad libitum*. Male Sprague Dawley rats (8–10 weeks old, Envigo) were used for spinal nerve ligation (SNL) to induce neuropathic pain as described previously (Kim and Chung, 1992). Briefly, rats were anesthetized with 2–3% isoflurane, and the left L5 and L6 spinal nerves were exposed and ligated with 6–0 silk sutures separately under a surgical microscope. Sham surgery (the same surgical procedure without nerve ligation) was used as the control.

Cacna2d1 KO mice were originally obtained from the Medical Research Council (stock #6900) and were generated as described

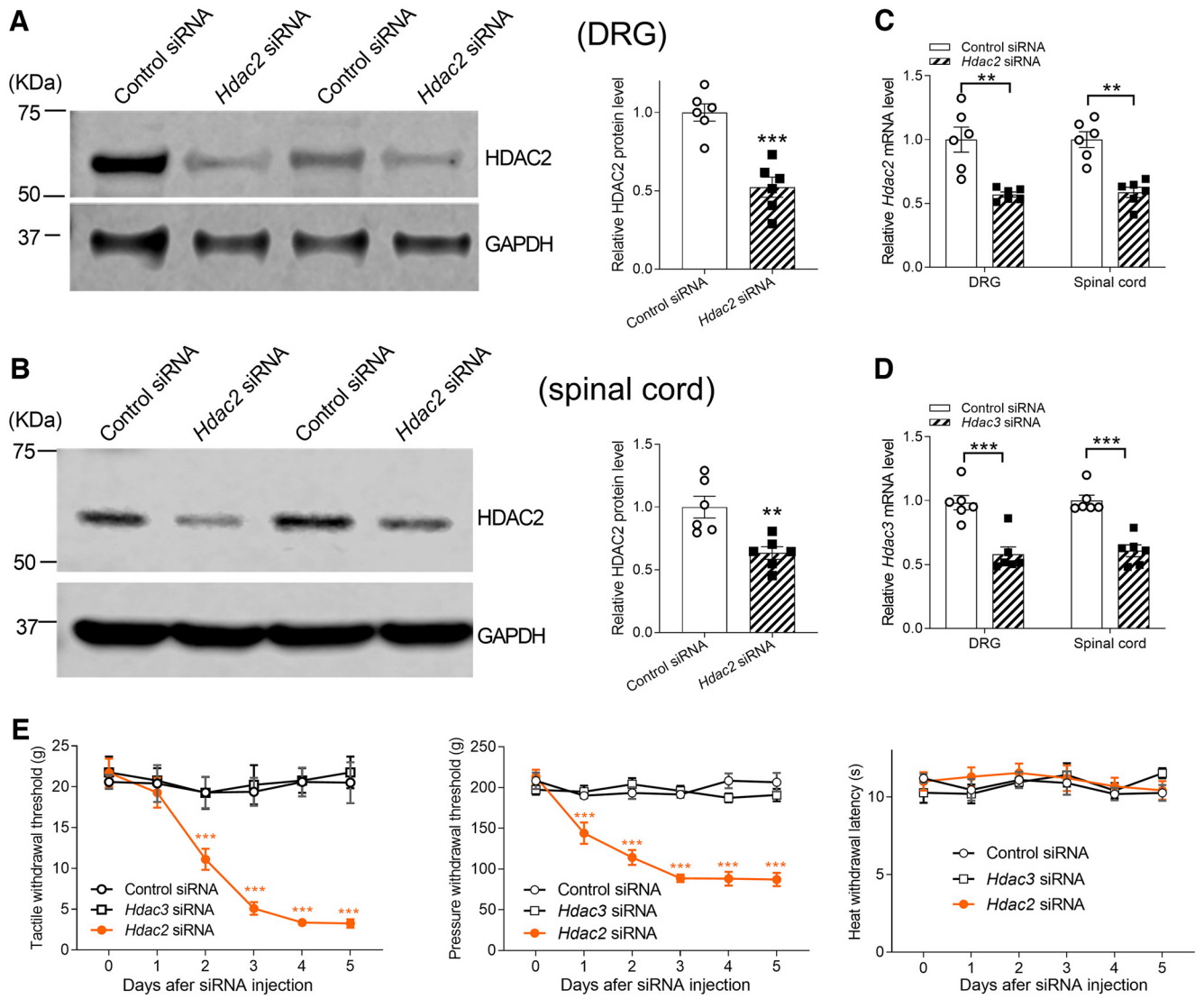

Figure 2. HDAC2 knockdown at the spinal cord level causes pain hypersensitivity. ***A***, ***B***, Representative blots and quantification show the protein levels of HDAC2 in the DRG (***A***) and spinal cord (***B***) of rats treated with control siRNA or *Hdac2*-specific siRNA; $^{**}p < 0.01$, $^{***}p < 0.001$, two-tailed *t* test, $n = 6$ rats per group. ***C***, ***D***, Quantitative PCR shows the mRNA levels of *Hdac2* (***C***) and *Hdac3* (***D***) in the DRG of rats treated with control siRNA, *Hdac2*-specific siRNA, or *Hdac3*-specific siRNA; $^{**}p < 0.01$, $^{***}p < 0.001$, two-tailed *t* test, $n = 6$ rats per group. ***E***, Time course of changes in withdrawal thresholds tested with von Frey filaments, pressure, and heat stimuli in rats treated with *Hdac2*-specific siRNA, *Hdac3*-specific siRNA, or control siRNA. Two-way ANOVA showed a significant interaction between the siRNA type and treatment time ($F_{(5,66)} = 13.47$, $p < 0.001$ for tactile threshold; $F_{(5,66)} = 15.75$, $p < 0.001$ for pressure threshold); $^{***}p < 0.001$, compared with baseline (day 0), two-way ANOVA with Tukey's *post hoc* test ($n = 6$ rats in control siRNA group, $n = 7$ rats in *Hdac2*-siRNA and *Hdac3*-siRNA groups). Data are expressed as means ± SEM.

previously (Fuller-Bicer et al., 2009). *Hdac2* conditional knockout (*Hdac2*-cKO) mice were generated by crossing female mice carrying LoxP recombination sites flanking exons 5 and 6 of the *Hdac2* gene ($Hdac2^{fl/fl}$; Guan et al., 2009; Wilting et al., 2010) and male mice with Advillin promotor-driven Cre-recombinase expression ($Avl^{Cre+/-}$; X. Zhou et al., 2010; da Silva et al., 2011). $Avl^{Cre+/-}$::$Hdac2^{fl/-}$ mice obtained from the first generation were crossed again with female $Hdac2^{fl/fl}$ mice to obtain $Avl^{Cre/+}$::$Hdac2^{fl/fl}$ (*Hdac2*-cKO mice).

To ablate the *Hdac2* gene from DRG neurons in adult mice, we crossed $Hdac2^{fl/fl}$ mice with tamoxifen-dependent inducible *Avl*-Cre^{ERT2} (stock #032027, The Jackson Laboratory; Lau et al., 2011). Tamoxifen (catalog #T5648, Sigma-Aldrich) was dissolved in corn oil (catalog #C8267, Sigma-Aldrich) and injected intraperitoneally (75 mg/kg/day for 5 consecutive days) to induce *Hdac2* deletion in DRG neurons in *Avl*-Cre^{ERT2}::$Hdac2^{fl/fl}$ mice (*Hdac2*-icKO). The Advillin Cre-induced target gene KO occurs in 87% of DRG neurons in *Avl*-Cre^{ERT2} mice (Woo et al., 2014) and in 84% of DRG neurons in the Avl^{Cre} line (Zappia et al., 2017). Both male and female adult mice (8–14 weeks of age) were used for electrophysiological and behavioral studies. Data were pooled from males and females because no evident sex difference was detected during the course of our study. After weaning (3 weeks after birth), mice were ear tagged and genotyped using ear tissues with PCR. Littermates without Cre were used as controls ($Hdac2^{fl/fl}$). Genotyping primers are listed in Table 1.

Intrathecal catheter placement and siRNA treatment. For intrathecal catheter implants, rats were anesthetized with 2–3% isoflurane. A small incision was made at the back of the neck, and a PE-10 catheter (8 cm) was inserted via a small opening made on the atlanto-occipital membrane of the cisterna magna so that the catheter tip reached the lumbar enlargement (Chen and Pan, 2001). The animals were allowed to recover for 5–7 d before intrathecal siRNA injections. Rat *Hdac2* siRNA (MISSION® siRNA Product, siRNA ID #SASI-RN02-00300570), rat *Hdac3* siRNA (MISSION® siRNA Product, siRNA ID #SASI-RN01-00031908), mouse *Hdac2* siRNA (MISSION® siRNA Product, siRNA ID #SASI_Mm01_00100699), and control siRNA (catalog #SIC001, MISSION siRNA Universal Negative Control #1) were obtained from Sigma-Aldrich. The sequence for rat *Hdac2* and rat *Hdac3* siRNA was GAUAUCGGGA

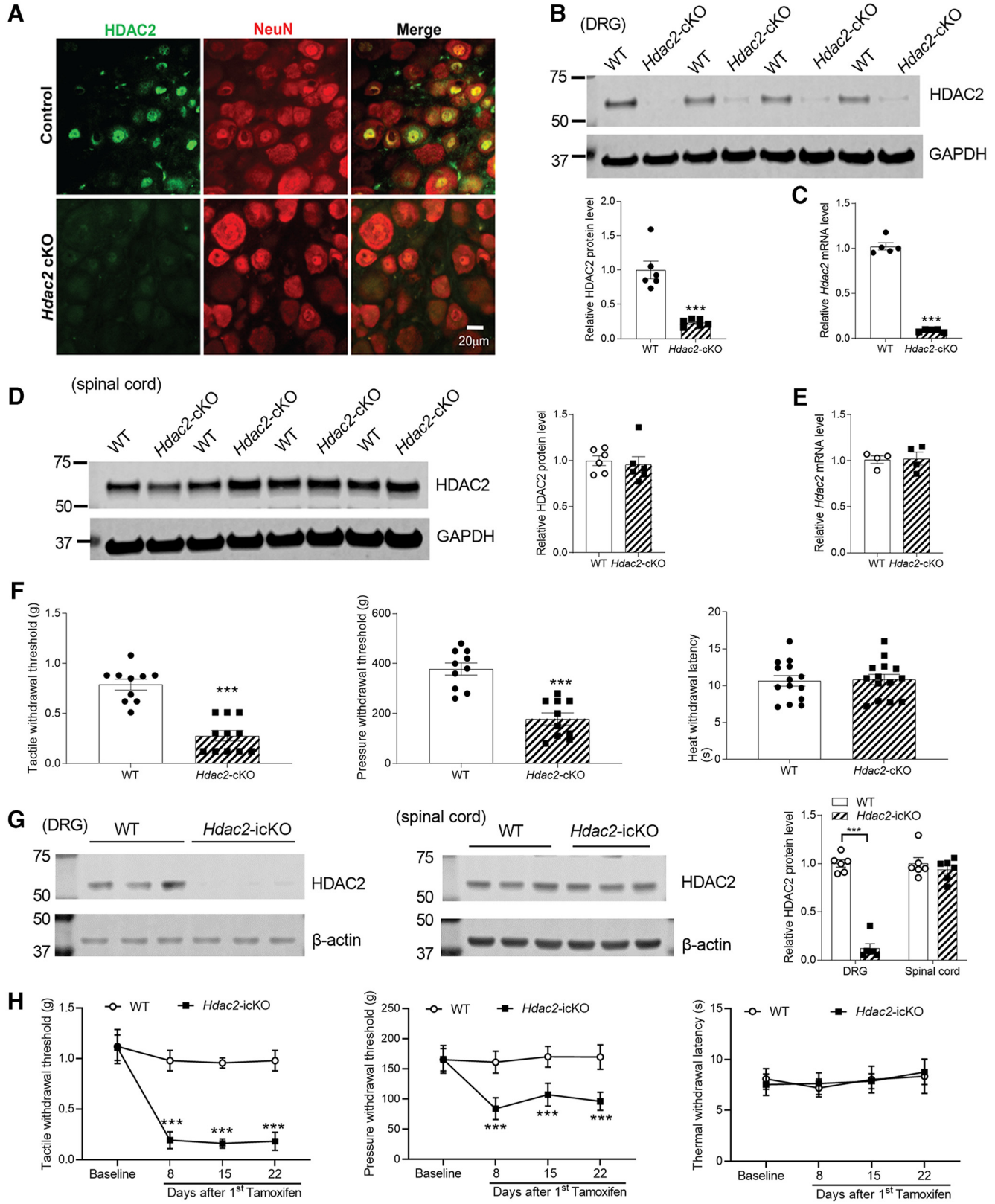

Figure 3. HDAC2 ablation in primary sensory neurons induces pain hypersensitivity. ***A***, Representative immunocytochemical labeling shows the presence of HDAC2 (green)- and NeuN (red)-labeled neurons in the DRG section from *Hdac2*-cKO and WT control mice. ***B***, Representative blots and quantification show the HDAC2 protein level in the DRG of *Hdac2*-cKO and WT mice; $^{***}p < 0.001$, two-tailed *t* test, $n = 6$ mice per group. ***C***, The mRNA level of *Hdac2* in the DRG of *Hdac2*-cKO and WT mice; $^{***}p < 0.001$, two-tailed *t* test, $n = 5$ mice per group. ***D***, Representative blots and quantification show the HDAC2 protein level in the spinal cord of *Hdac2*-cKO and WT mice, $n = 6$ mice per group. ***E***, The mRNA level of *Hdac2* in the spinal cord of *Hdac2*-cKO and WT mice, $n = 4$ mice per group. ***F***, Withdrawal thresholds tested with von Frey filaments, pressure, and heat stimuli in 10-week-old *Hdac2*-cKO mice and WT mice; $^{***}p < 0.001$, two-tailed *t* test ($n = 10$ WT mice, $n = 11$ *Hdac2*-cKO mice for von Frey filament test; $n = 10$ mice per group for pressure test; $n = 14$ mice per group for heat test). ***G***, Representative blots and quantification show the HDAC2 protein level in the DRG and spinal cord of *Avil-Cre*$^{ERT2/+}$::*Hdac2*$^{fl/fl}$ (*Hdac2*-icKO) and WT mice treated with tamoxifen; $^{***}p < 0.001$, two-tailed *t*

AUUAUUAUU[dT][dT] and GAGUUCUGCUCCCGCUAUA[dT][dT], respectively.

The sequence for mouse *Hdac2* siRNA was CUGCUAAAUUA UGGUUUAU[dT][dT]. i-Fect (catalog #NI35150, Neuromics) was used to dissolve and deliver the siRNA via intrathecal injection, as we described previously (Laumet et al., 2015; Zhang et al., 2018). Intrathecal injection in mice was performed using a lumbar puncture technique, as previously described (Huang et al., 2020; Zhang et al., 2021). A mixture of 2 μg of siRNA in 10 μl of i-Fect was intrathecally injected daily for 5 consecutive days.

Nociceptive behavioral tests. For measurement of tactile sensitivity, mice or rats were habituated on a wire-grid panel for 30 min before testing. A series of von Frey filaments (Stoelting) was applied to the plantar surface of the hindpaw. A quick withdrawal or flinching of the paw was considered a positive response. In the absence of a response, we applied the filament of the next greater force. We used the up-down method to calculate the tactile threshold that produced a 50% likelihood of a withdrawal response as previously described (Chaplan et al., 1994).

For measurement of mechanical nociception in rats, we used an analgesiometer (Ugo Basile) to perform the paw pressure test. A foot pedal was pressed to activate a motor that applied a linearly increasing force to the dorsal surface of the hindpaws. The pedal was immediately released when the animal displayed pain by either withdrawing the paw or vocalizing. Each trial was repeated two or three times at 2 min intervals, and the mean value was used as the force needed to produce a withdrawal response (Chen et al., 2014b, 2018). To quantify the pressure withdrawal threshold in mice, we used a Pincher Analgesia Meter (model 2450, IITC Life Science) to apply pressure with increasing force on the midplantar glabrous surface of hindpaws as previously described (Zhang et al., 2018; Jin et al., 2022). Brisk withdrawal or vocalization was considered a positive response and recorded as the withdrawal threshold. The cutoff was set to 400 g to minimize potential tissue injury.

For measurement of heat sensitivity, mice or rats were tested on a Plantar Analgesia Meter (model 400, IITC Life Science). The plantar surface was maintained at 30°C, and animals were habituated for 30 min before each test. A mobile radiant heat stimulus was applied to the plantar surface of the hindpaw until the animal displayed a withdrawal response or paw licking, as described previously (Chen et al., 2014a, b). The cutoff was set to be 30 s to minimize potential tissue injury.

Immunoblotting. Total proteins were extracted from the lumbar DRG and dorsal spinal cord tissues (at L5/L6 levels in rats and L3–L5 levels in mice) using an extraction buffer (50 mM Tris-HCl, pH 7.4, 1% NP-40, 1% sodium deoxycholate, 150 mM NaCl, 1 mM EDTA, 1 mM Na_3VO_4, and 1 mM NaF in the presence of a proteinase inhibitor cocktail; Sigma-Aldrich). In the same experiments, synaptosomes were prepared from dorsal spinal cords at L3–L5 levels in mice, as described previously (Chen et al., 2018; Chen et al., 2019). In brief, tissues were gently homogenized with 15 slow strokes using glass homogenizer in 2 ml of ice-cold Syn-PER reagent (Thermo Fisher Scientific) containing a protease inhibitor cocktail (Sigma-Aldrich). The homogenate was centrifuged at 1200 × *g* for 10 min at 4°C to remove the nuclei and large debris. The supernatant was centrifuged at 15,000 × *g* for 20 min at 4°C to obtain the synaptosome pellet. The pellet was then dissolved in RIPA buffer (Thermo Fisher Scientific) containing a protease inhibitor cocktail and centrifuged at 15,000 × *g* for 10 min at 4°C to obtain the synaptosomal protein in the supernatant.

The protein was quantified using a DC protein assay kit (Bio-Rad). A quantity of 30 μg of protein from each sample was loaded and separated on 4–12% Bis-Tris SDS-PAGE gel (Invitrogen). The primary antibodies used for immunoblotting are listed in Table 2. The protein bands were detected with an enhanced chemiluminescence kit (Thermo Fisher Scientific), and the protein band density was visualized and quantified using an Odyssey Fc Imager (LI-COR Biosciences).

Immunohistochemistry. Mice were deeply anesthetized with sodium pentobarbital (60 mg/kg, i.p.) and perfused with PBS and then 4% paraformaldehyde in 0.1 M PBS. The DRG was dissected, postfixed for 2 h with 4% paraformaldehyde followed sequentially by 10, 20, and 30% sucrose solutions in PBS, and frozen in Tissue-Tek optimal cutting temperature compound. Slices were cut to 20 μm thick, collected onto SuperFrost Plus glass slides, and air dried for 1 h at 25°C. After washing with PBS, the sections were incubated in a blocking solution containing 1% bovine serum albumin in PBS for 20 min, incubated with the primary antibodies overnight at 4°C, and then incubated with the corresponding secondary antibodies conjugated to Alexa Fluor 488 or Alexa Fluor 568 (1:200; Invitrogen) for 1 h at 25°C. The primary antibodies used for immunocytochemistry are listed in Table 2. Images were acquired with a confocal laser-scanning microscope (Zeiss).

RNA sequencing. An RNA-sequencing library was constructed using RNAs from the mouse L3–L5 DRGs and sequenced using the Illumina Platform with paired-end reads (150 bp, mean 20 million reads) per sample (Novogene). Reads were mapped to the mouse genome (mm10) using Hisat2 (Kim et al., 2015). The mapped files were converted and sorted into BAM files using samtools (Li et al., 2009). Then the reads of each gene were calculated using featureCounts (Liao et al., 2014). Differentially expressed genes were analyzed using DESeq2 (Love et al., 2014). Gene Ontology (GO) Enrichment Analysis was performed using PANTHER online software (Mi et al., 2019). Pathway enrichment of differentially expressed genes was analyzed using Ingenuity Pathway Analysis (Krämer et al., 2014). Raw sequencing datasets have been deposited in the Gene Expression Omnibus (accession no. GSE145125).

Quantitative PCR. Total RNAs were extracted from the lumbar DRG and dorsal spinal cord tissues using TRIsure (catalog #BIO-38 032, BioLine). Samples were treated with RNase-free DNase (catalog #79254, QIAGEN), and 1 μg of RNA was used for reverse-transcription with a RevertAid RT Reverse Transcription Kit (catalog #K1691, Thermo Fisher Scientific). A total of 2 μl of five-times diluted cDNA was added to a 20 μl reaction volume with SYBR Green Real-Time PCR Mix (catalog #A25780, Thermo Fisher Scientific). Real-time PCR was run on a QuantStudio 7 Flex Real-Time PCR System (Applied Biosystems). The thermal cycling conditions were as follows: 95°C for 10 min, 40 cycles of 95°C for 15 s, and 60°C for 45 s (Zhang et al., 2018; Ghosh et al., 2022). The primers used are listed in Table 1.

Chromatin immunoprecipitation. Chromatin immunoprecipitation (ChIP) assays were performed as previously described (Zhang et al., 2016; Zhang et al., 2018; Ghosh et al., 2022). Briefly, lumbar DRG tissues (L3–L5 in mice and L5/L6 in rats) were isolated and cross-linked with 2% formaldehyde for 10 min at 25°C. The crossed tissues were lysed with lysis buffer and sonicated to fragments of 200–1000 bp using a water bath sonicator (Qsonica) at 4°C (40 cycles, 30 s on and 30 s off). Chromatin was pulled down using the magnetic beads Dynabeads Protein G (catalog #10003D, Thermo Fisher Scientific) conjugated with indicated antibodies listed in Table 2. After de-cross-linking, DNA was recovered using a QIAquick PCR Purification Kit (catalog #28104, Qiagen). Data were analyzed and corrected by input (10% of the amount used for ChIP) or H3. Primers used for the ChIP assay are listed in Table 1.

Electrophysiological recordings in spinal cord slices. The lumbar spinal cord was obtained through laminectomy in mice anesthetized with 3% isoflurane. Spinal cords were placed in ice-cold artificial CSF containing the following (in mM): 234 sucrose, 3.6 KCl, 1.2 $MgCl_2$, 2.5 $CaCl_2$, 1.2 NaH_2PO_4, 12 glucose, and 25 $NaHCO_3$, presaturated with 95% O_2 and 5% CO_2. Transverse slices were cut to 400 μm thick in ice-cold artificial CSF using a vibratome. The slices were preincubated in Krebs solution containing the following (in mM): 117 NaCl, 3.6 KCl, 1.2 $MgCl_2$, 2.5 $CaCl_2$, 1.2 NaH_2PO_4, 11 glucose, and 25 $NaHCO_3$, oxygenated with 95% O_2 and 5% CO_2 at 34°C for at least 1 h. The slices were transferred into a glass-bottom recording chamber

←

test, $n = 6$ mice per group. ***H***, Time course of changes in withdrawal thresholds tested with von Frey filaments, pressure, and heat stimuli in tamoxifen-induced *Hdac2*-icKO and WT mice. Two-way ANOVA showed a significant interaction between the genotype and treatment time ($F_{(3,40)} = 44.7$, $p < 0.001$ for tactile threshold; $F_{(3,40)} = 11.04$, $p < 0.001$ for pressure threshold); ***$p < 0.001$, compared with baseline, two-way ANOVA with Tukey's *post hoc* test; $n = 5$ WT mice, $n = 7$ *Hdac2*-icKO mice. Data are expressed as means ± SEM.

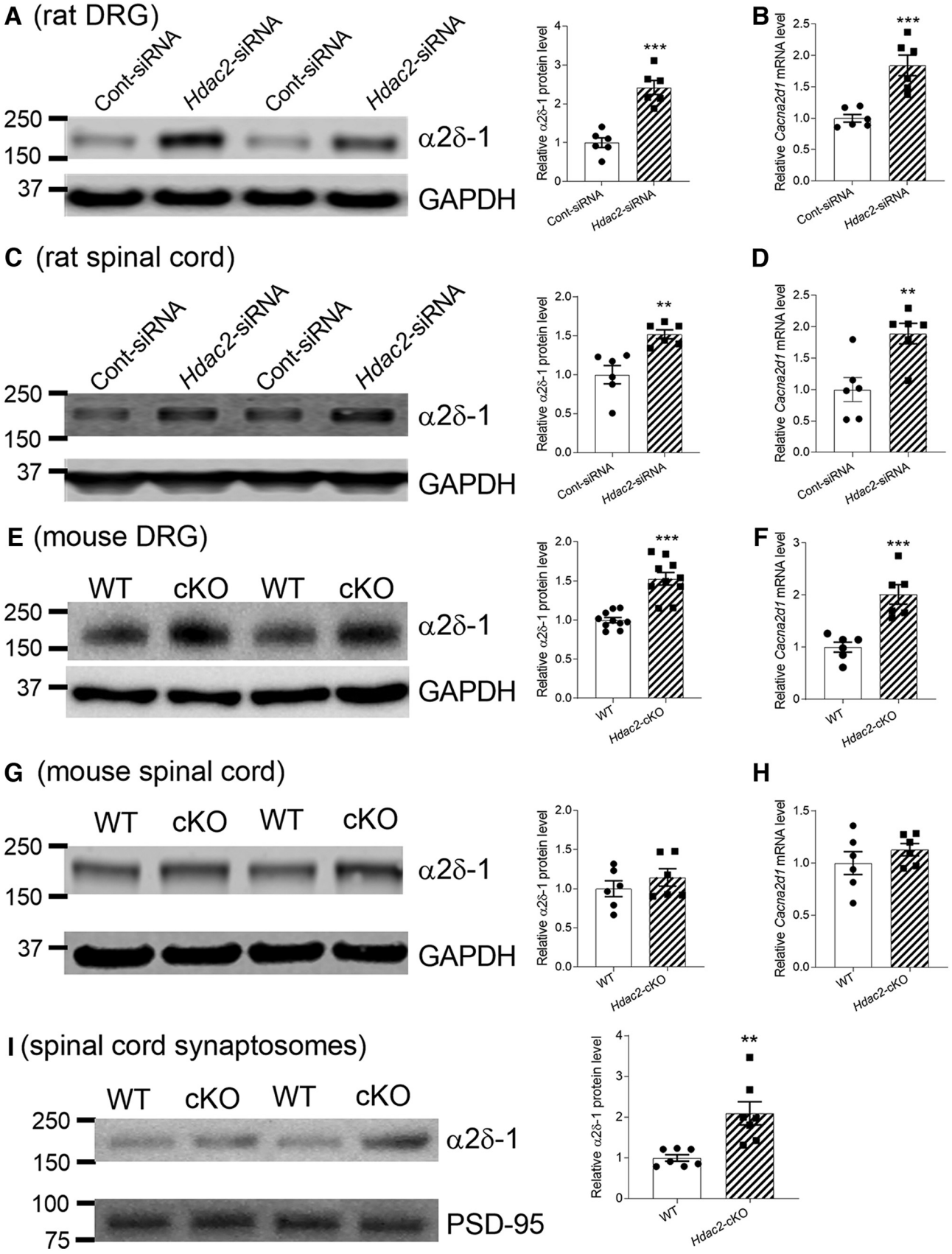

Figure 4. HDAC2 deficiency increases $\alpha2\delta$-1 expression in the DRG and spinal cord. ***A***, ***B***, Representative blots and quantification (***A***) and quantitative PCR (***B***) show the protein and mRNA levels of $\alpha2\delta$-1 in the DRG from *Hdac2*-specific siRNA- or control siRNA-treated rats; $^{***}p < 0.001$, two-tailed *t* test, $n = 6$ rats per group. ***C***, ***D***, Representative blots and quantification (***C***) and quantitative PCR (***D***) show the protein and mRNA levels of $\alpha2\delta$-1 in the spinal cord from *Hdac2*-specific siRNA-treated or control siRNA-treated rats; $^{**}p < 0.01$, two-tailed *t* test, $n = 6$ rats per group. ***E***, ***F***, Representative blots and quantification (***E***, $n = 10$ mice) and quantitative PCR (***F***, $n = 6$ mice) show the protein and mRNA levels of $\alpha2\delta$-1 in the DRG from *Hdac2*-cKO or

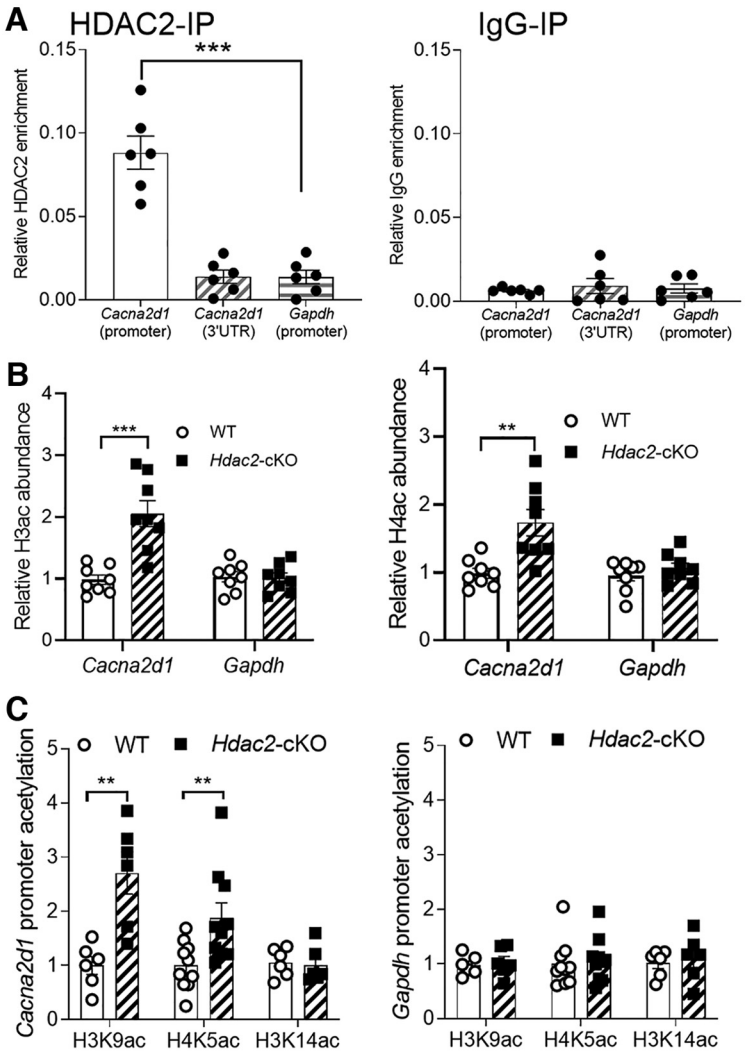

Figure 5. HDAC2 in primary sensory neurons restrains histone acetylation at the *Cacna2d1* promoter in the DRG. ***A***, The occupancy of HDAC2 at the promoter region (71 to 164 bp) of *Cacna2d1* in the mouse DRG. The 3′ untranslated region (UTR; 440,221 to 440,390 bp) of *Cacna2d1* and promoter of *Gapdh* (−53 to 85 bp) were used as controls. IgG was used as a negative control for HDAC2 immunoprecipitation (HDAC2-IP); $^{***}p < 0.001$, one-way ANOVA with Tukey's *post hoc* test, $n = 6$ mice per group. ***B***, Total H3ac and H4ac levels at the *Cacna2d1* and *Gapdh* promoters in the DRG from *Hdac2*-cKO and WT mice; $^{**}p < 0.01$, $^{***}p < 0.001$, two-tailed *t* test; $n = 8$ mice per group. ***C***, The H3K9ac, H4K5ac, and H3K14ac levels at the *Cacna2d1* and *Gapdh* promoters in the DRG from *Hdac2*-cKO and WT mice; $^{**}p < 0.01$, two-tailed *t* test; $n =$ 6 mice per group for H3K9ac and H3K14ac, $n = 10$ mice per group for H4K5ac. Data are expressed as means ± SEM.

(Warner Instruments) and perfused continuously with Krebs solution at 3 ml/min at 34°C.

Neurons from the lamina II outer zone were selected for whole-cell patch-clamp recordings because they are involved in processing nociceptive input from primary afferent nerves (Li et al., 2002; Santos et al., 2007; Wang et al., 2018). A glass pipette (5–10 MΩ) was filled with an internal solution containing the following (in mM): 135 potassium gluconate, 5 tetraethylammonium chloride, 2 $MgCl_2$, 0.5 $CaCl_2$, 5 HEPES, 5 EGTA, 5 Mg-ATG, 0.5 Na-GTP, 1 guanosine 5'-O-(2-thiodiphosphate) trilithium salt, and 10 lidocaine *N*-ethyl bromide, pH adjusted to 7.2–7.4, with 1 M KOH and osmotic pressure to 290–300 mOsmol. EPSCs were elicited by electrical stimulation (0.2 ms, 0.6 mA, and 0.1 Hz) of the dorsal root and recorded at a holding potential of −60 mV. Monosynaptic EPSCs were identified on the basis of the constant latency and absence of conduction failure of evoked EPSCs in response to a 20 Hz electrical stimulation (Li et al., 2002; H.Y. Zhou et al., 2010; Chen et al., 2018). For paired-pulse stimulation, two EPSCs were electrically evoked by a pair of stimuli given at 50 ms intervals. The paired-pulse synaptic response, a measure of presynaptic plasticity, was expressed as the ratio of the amplitude of the second EPSC to the amplitude of the first EPSC (H.Y. Zhou et al., 2010; Xie et al., 2016).

To measure quantal glutamate release from presynaptic terminals, miniature EPSCs (mEPSCs) were recorded from lamina II outer neurons in the presence of 0.5 μM tetrodotoxin at a holding potential of −60 mV (Li et al., 2002; Chen et al., 2014a). The input resistance was continuously monitored, and the recording was terminated if the input resistance changed by >15%. Signals were recorded using an amplifier (MultiClamp 700B, Molecular Devices), filtered at 1–2 kHz, digitized at 10 kHz, and stored for off-line analysis. All drugs were freshly prepared in artificial CSF before the experiments and delivered via syringe pumps to reach their final concentrations. Tetrodotoxin (catalog #HB1035) and 2-amino-5-phosphonopentanoic acid (AP5; catalog #HB0252) were purchased from Hello Bio.

Study design and statistical analysis. Data are presented as means ± SEM. Data collection was randomized, and the investigators performing behavioral tests and electrophysiological recordings were blinded to the genotype and treatment. In electrophysiological experiments, only one neuron was recorded from each spinal cord slice, and at least five animals were used for each group. The amplitude of the evoked EPSCs was quantified by averaging 10 consecutive EPSCs with Clampfit 10.0 software (Molecular Devices). The amplitude and frequency of mEPSCs were analyzed using the MiniAnalysis peak detection program (Synaptosoft). The cumulative probability of the amplitude and the interevent interval of the mEPSCs were compared using the Kolmogorov–Smirnov test, which estimates the probability that two distributions are similar (Li et al., 2010; Chen et al., 2014b). RNA-sequencing data were generated using DRG tissues from wild-type (WT) and *Hdac2*-cKO mice in triplicates, and differentially expressed genes were identified by setting the threshold at $p < 0.05$. The Student's *t* test was used to compare two groups. We used one-way and two-way ANOVAs to compare more than two groups. Statistical analysis was performed using GraphPad Prism (version 8) software; $p < 0.05$ was considered to be statistically significant.

Results

Nerve injury increases histone acetylation and diminishes HDAC2 enrichment at the *Cacna2d1* promoter in the DRG

As a first step toward understanding how $\alpha2\delta$-1 expression is controlled by epigenetic mechanisms, we determined whether histone acetylation levels at the *Cacna2d1* promoter in the DRG are altered by nerve injury. We performed L5 and L6 SNL in rats, a well-characterized animal model of chronic neuropathic

←

WT mice; $^{***}p < 0.001$, two-tailed *t* test. ***G***, ***H***, Representative blots and quantification (***G***) and quantitative PCR (***H***) show the protein and mRNA levels of $\alpha2\delta$-1 in the spinal cord from *Hdac2*-cKO or WT mice; $n = 6$ mice per group. ***I***, Representative blots and quantification show the $\alpha2\delta$-1 protein level in dorsal spinal cord synaptosomes from *Hdac2*-cKO or WT mice; $^{**}p < 0.01$, two-tailed *t* test, $n = 7$ mice per group. Data are expressed as means ± SEM.

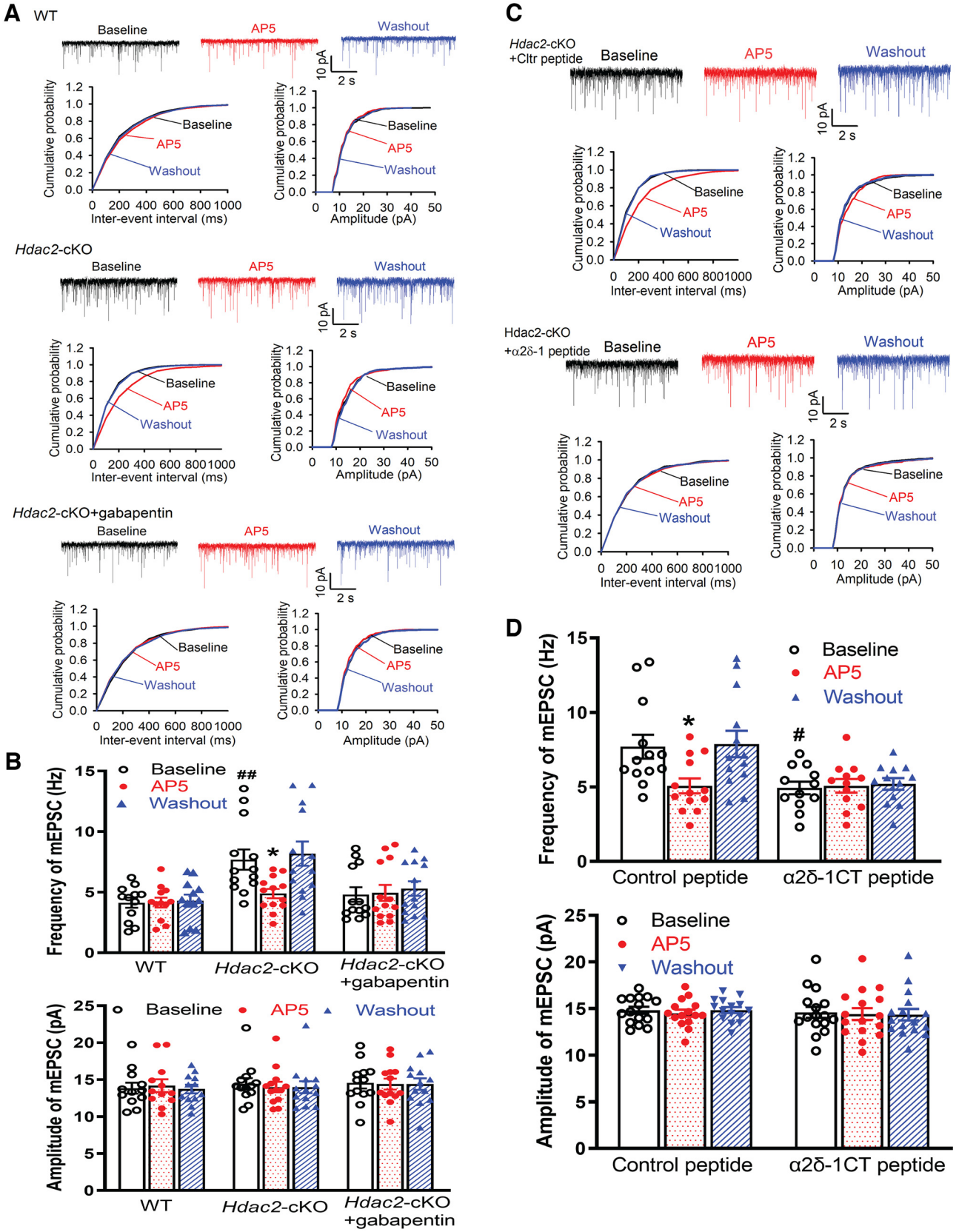

Figure 6. HDAC2 in DRG neurons constitutively restrains $\alpha 2\delta$-1–dependent presynaptic NMDAR activity in the spinal dorsal horn. ***A***, ***B***, Representative current traces and cumulative plots (***A***) and mean changes (***B***) of mEPSCs of spinal lamina II neurons before (Baseline), with (AP5), and after (Washout) bath application of 50 μM AP5. Slice recordings were performed using spinal cords from five WT mice ($n = 12$ neurons), six *Hdac2*-cKO mice ($n = 13$ neurons), and five *Hdac2*-cKO mice pretreated with 100 μM gabapentin ($n = 13$ neurons). Two-way ANOVA (***B***) showed there was a significant main effect for AP5 treatment ($F_{(2,69)} = 26.34$, $p < 0.001$) and a significant interaction between the genotype and AP5 treatment ($F_{(2,69)} = 3.497$, $p = 0.0358$). ***C***, ***D***, Original recording traces and cumulative plots (***C***) and mean changes (***D***) show the effect of pretreatment with Tat-fused $\alpha 2\delta$-1CT peptide or control peptide on the frequency and amplitude of mEPSCs of spinal lamina II neurons before (Baseline), with (AP5), and after (Washout) bath application of 50 μM AP5. Spinal cords slices were obtained from *Hdac2*-cKO mice and pretreated

pain (Kim and Chung, 1992). ChIP and quantitative PCR (ChIP-PCR) assays using DRGs removed from rats 3 weeks after surgery showed that SNL significantly increased the acetylation levels of histone H3 and H4 at the promoter region of *Cacna2d1* [$p = 0.0012$, $t_{(9)} = 3.825$ for H3 acetylation (H3ac); $p = 0.0083$, $t_{(9)} = 3.366$ for H4 acetylation (H4ac); Fig. 1*A*] but not the housekeeping gene *Gapdh*. Furthermore, SNL significantly increased the levels of H3K9 acetylation (H3K9ac; $p = 0.0009$, $t_{(5)} = 6.807$) and H4K5 acetylation (H4K5ac; $p = 0.0013$, $t_{(8)} = 3.353$), two histone marks associated with active gene transcription (Guan et al., 2009; Laumet et al., 2015), at the *Cacna2d1* promoter in the DRG (Fig. 1*B*).

Among the four subtypes of Class I HDACs (HDAC1, HDAC2, HDAC3, and HDAC8), HDAC2 is the most abundant subtype expressed in DRG neurons and is upregulated in the injured DRG (Laumet et al., 2015). HDAC3 is also expressed in DRG neurons and plays a role in axonal regeneration (Hervera et al., 2019). In contrast, HDAC1 is mainly present in glial cells, and HDAC8 is minimally expressed in the DRG (Laumet et al., 2015). Thus, we next used the ChIP-PCR assay to determine whether nerve injury affects the occupancy of HDAC2 and HDAC3 at the *Cacna2d1* promoter. Remarkably, our promoter occupancy assay showed that SNL caused a large reduction in the enrichment of HDAC2 at the *Cacna2d1* promoter ($p < 0.002$, $t_{(5)} = 9.814$; Fig. 1*C*). However, the enrichment of HDAC3 at the *Cacna2d1* promoter in the DRG did not differ significantly between SNL and sham control groups (Fig. 1*D*). These data raised the possibility that nerve injury increases *Cacna2d1* transcription in the DRG by diminishing HDAC2 binding and consequent histone hyperacetylation at the *Cacna2d1* promoter.

HDAC2, but not HDAC3, constitutively inhibits mechanical pain hypersensitivity

Because HDAC2 enrichment at the *Cacna2d1* promoter in the DRG is diminished by nerve injury, we next used loss-of-function analysis to determine the role of constitutive HDAC2 in regulating pain hypersensitivity. We first used siRNA-induced HDAC2 knockdown to define the role of HDAC2 at the spinal cord level in the control of nociception. Intrathecal injection of *Hdac2*-specific siRNA in rats for 5 d caused ~50% reduction in HDAC2 expression levels in the DRG and dorsal spinal cord (Fig. 2*A–C*). Strikingly, treatment with *Hdac2*-specific siRNA, but not the control siRNA, gradually and profoundly reduced the hindpaw withdrawal thresholds in response to tactile and noxious pressure stimuli ($p < 0.0001$, $F_{(5,66)} = 11.42$ for tactile threshold; $p < 0.0001$, $F_{(5,66)} = 17.62$ for pressure threshold; Fig. 2*E*). Treatment with *Hdac2*-specific siRNA did not significantly alter the heat withdrawal latency (Fig. 2*E*). In contrast, treatment with *Hdac3*-specific siRNA for 5 d had no significant effects on the tactile, pressure, or heat withdrawal threshold in rats (Fig. 2*D*,*E*).

To specifically determine the role of HDAC2 in primary sensory neurons in nociceptive control, we generated *Hdac2* conditional knockout (*Hdac2*-cKO, $Avl^{Cre/+}$::$Hdac2^{fl/fl}$) mice by crossing $Hdac2^{fl/fl}$ mice (Guan et al., 2009) with $Avl^{Cre/+}$ mice (X. Zhou et al., 2010) so that *Hdac2* in DRG neurons was selectively ablated (Fig. 3*A–E*). Consistent with rats treated with *Hdac2*-specific siRNA, the tactile and pressure withdrawal thresholds were much lower in *Hdac2*-cKO mice than in age-matched littermate WT controls ($p < 0.0001$, $t_{(19)} = 6.881$ for tactile threshold; $p < 0.0001$, $t_{(18)} = 5.852$ for pressure threshold; Fig. 3*F*). However, the heat-elicited withdrawal latency was similar between *Hdac2*-cKO and WT mice (Fig. 3*F*).

Because deletion of *Hdac2* in premature mice may affect DRG neuronal development, we generated mice with tamoxifen-dependent inducible deletion of *Hdac2* in DRG neurons by crossing $Hdac2^{fl/fl}$ mice with Advillin-Cre^{ERT2} mice (Lau et al., 2011). We used tamoxifen treatment to induce *Hdac2* conditional KO in DRG neurons in adult *Avl*-Cre^{ERT2}::$Hdac2^{fl/fl}$ mice (*Hdac2*-icKO; Fig. 3*G*). Before tamoxifen treatment, the tactile, pressure, and heat withdrawal thresholds were similar between *Avl*-Cre^{ERT2}::$Hdac2^{fl/fl}$ and WT mice. Tamoxifen treatment had no effect on the tactile, pressure, or heat withdrawal thresholds in WT control mice (Fig. 3*H*). In contrast, *Hdac2*-icKO mice showed profoundly reduced tactile and pressure withdrawal thresholds, and these reductions lasted at least 3 weeks ($p < 0.0001$, $F_{(3,40)} = 84.92$ for tactile threshold; $p < 0.0001$, $F_{(3,40)} = 11.16$ for pressure threshold; Fig. 3*H*). The heat withdrawal latency did not differ significantly between *Hdac2*-icKO and WT mice (Fig. 3*H*). Together, these findings reveal a crucial role of constitutive HDAC2 in primary sensory neurons in suppressing mechanical pain hypersensitivity.

HDAC2 in primary sensory neurons tonically inhibits *Cacna2d1* transcription and histone acetylation at the *Cacna2d1* promoter

In subsequent experiments, we used loss-of-function approaches to determine the role of constitutively expressed HDAC2 in the DRG in regulating $\alpha2\delta$-1 expression. Increased $\alpha2\delta$-1 expression at the spinal cord level increases both presynaptic and postsynaptic NMDAR activity in the spinal dorsal horn (Chen et al., 2018). We first used quantitative PCR and immunoblotting to determine whether siRNA-induced *Hdac2* knockdown at the spinal cord level in rats alters $\alpha2\delta$-1 expression. Indeed, the mRNA ($p = 0.0007$, $t_{(10)} = 4.838$ for DRG; $p = 0.0054$, $t_{(10)} = 3.537$ for spinal cord) and protein ($p < 0.0001$, $t_{(10)} = 6.463$ for DRG; $p = 0.0026$, $t_{(10)} = 3.994$ for spinal cord) levels of $\alpha2\delta$-1 in DRG and dorsal spinal cord tissues were significantly greater in rats intrathecally treated with *Hdac2*-specific siRNA than in rats treated with control siRNA (Fig. 4*A–D*).

We also measured $\alpha2\delta$-1 expression in the DRG obtained from WT and *Hdac2*-cKO mice. The mRNA and protein levels of $\alpha2\delta$-1 in the DRG were much higher in *Hdac2*-cKO mice than in WT mice ($p = 0.0007$, $t_{(10)} = 4.822$ for mRNA levels; $p < 0.0001$, $t_{(18)} = 6.127$ for protein levels; Fig. 4*E*,*F*). Although the total protein and mRNA levels of $\alpha2\delta$-1 in the spinal cord did not differ significantly between WT and *Hdac2*-cKO mice, the $\alpha2\delta$-1 protein level in dorsal spinal cord synaptosomes was significantly greater in *Hdac2*-cKO than in WT mice ($p = 0.003$, $t_{(12)} = 3.707$; Fig. 4*G–I*). These results suggest that HDAC2 constitutively represses $\alpha2\delta$-1 expression in DRG neurons and their central terminals in the spinal dorsal horn.

We then used ChIP-PCR to determine the occupancy of HDAC2 in the *Cacna2d1* genomic sequence in the mouse DRG. HDAC2 was highly enriched at the promoter region (71–164 bp) of *Cacna2d1*, near its transcriptional start site ($p < 0.0001$, $F_{(2,15)} = 42.05$; Fig. 5*A*). However, HDAC2 was

←

with 1 μM $\alpha2\delta$-1CT peptide ($n = 12$ neurons from 5 mice) or 1 μM control peptide ($n = 13$ neurons from 6 mice).Two-way ANOVA (***D***) showed there was a significant main effect for AP5 treatment ($F_{(2,69)} = 3.441$, $p < 0.0376$) and a significant interaction between the control peptide and $\alpha2\delta$-1CT peptide treatment ($F_{(2,69)} = 3.239$, $p = 0.0452$); $^{*}p < 0.05$ versus respective baseline; $^{\#}p < 0.05$, $^{\#\#}p < 0.01$ versus the baseline in the WT or control peptide group, two-way ANOVA followed by Tukey's *post hoc* test. Data are expressed as means ± SEM.

not enriched at the 3′-untranscribed region (440,221 to 440,390 bp) of *Cacna2d1* (Fig. 5*A*). Also, there was no enrichment of HDAC2 at the promoter region of *Gapdh* in the DRG (Fig. 5*A*).

We next determined whether constitutive HDAC2 controls histone acetylation at the *Cacna2d1* promoter in the DRG. ChIP-PCR assays showed that the total H3 and H4 acetylation levels at the promoter of *Cacna2d1* ($p = 0.0003$, $t_{(14)} = 4.759$ for H3ac; $p = 0.0031$, $t_{(14)} = 3.563$ for H4ac), but not of *Gapdh,* in the DRG were much greater in *Hdac2*-cKO mice than in WT control mice (Fig. 5*B*). Furthermore, we determined which specific histone acetylation marks at the promoter of *Cacna2d1* are the substrates of HDAC2 in the DRG. We selected three histone acetylation marks, H3K9ac, H3K14ac, and H4K5ac, because they are generally associated with active gene transcription in neural tissues (Guan et al., 2009; Laumet et al., 2015; Yamakawa et al., 2017). The levels of H3K9ac ($p = 0.0024$, $t_{(10)} = 4.032$) and H4K5ac ($p = 0.0099$, $t_{(18)} = 2.885$) at the promoter of *Cacna2d1*, but not of *Gapdh,* in the DRG were significantly higher in *Hdac2*-cKO than in WT mice (Fig. 5*C*). However, the H3K14ac level at the *Cacna2d1* promoter in the DRG did not differ significantly between *Hdac2*-cKO and WT mice (Fig. 5*C*). Collectively, these data indicate that constitutive HDAC2 in DRG neurons is a key epigenetic repressor that inhibits *Cacna2d1* transcription by reducing histone acetylation at the promoter of *Cacna2d1*.

Constitutive HDAC2 in DRG neurons restrains activity of presynaptic NMDARs in the spinal dorsal horn by limiting α2δ-1 expression

α2δ-1 is essential for increased activity of presynaptic NMDARs at primary afferent central terminals in neuropathic pain conditions (Chen et al., 2018; Chen et al., 2019; Zhang et al., 2021). Based on this knowledge, we next sought to determine whether HDAC2 expressed in DRG neurons constitutively suppresses presynaptic NMDAR activity in the spinal dorsal horn. We performed whole-cell voltage-clamp recordings of mEPSCs of lamina II neurons in spinal cord slices from *Hdac2*-cKO and WT mice. The frequency, but not the amplitude, of mEPSCs of lamina II neurons was significantly greater in *Hdac2*-cKO mice than in WT mice ($p = 0.0058$, $n = 12$ neurons in WT group, $n = 13$ neurons in *Hdac2*-cKO group; Fig. 6*A*,*B*). This increased frequency of mEPSCs in *Hdac2*-cKO mice was abolished within 5 min after bath application of 50 μM AP5, a specific NMDAR antagonist. Similarly, pretreatment of spinal cord slices from *Hdac2*-cKO mice with 100 μM gabapentin, an α2δ-1 inhibitory ligand (Gee et

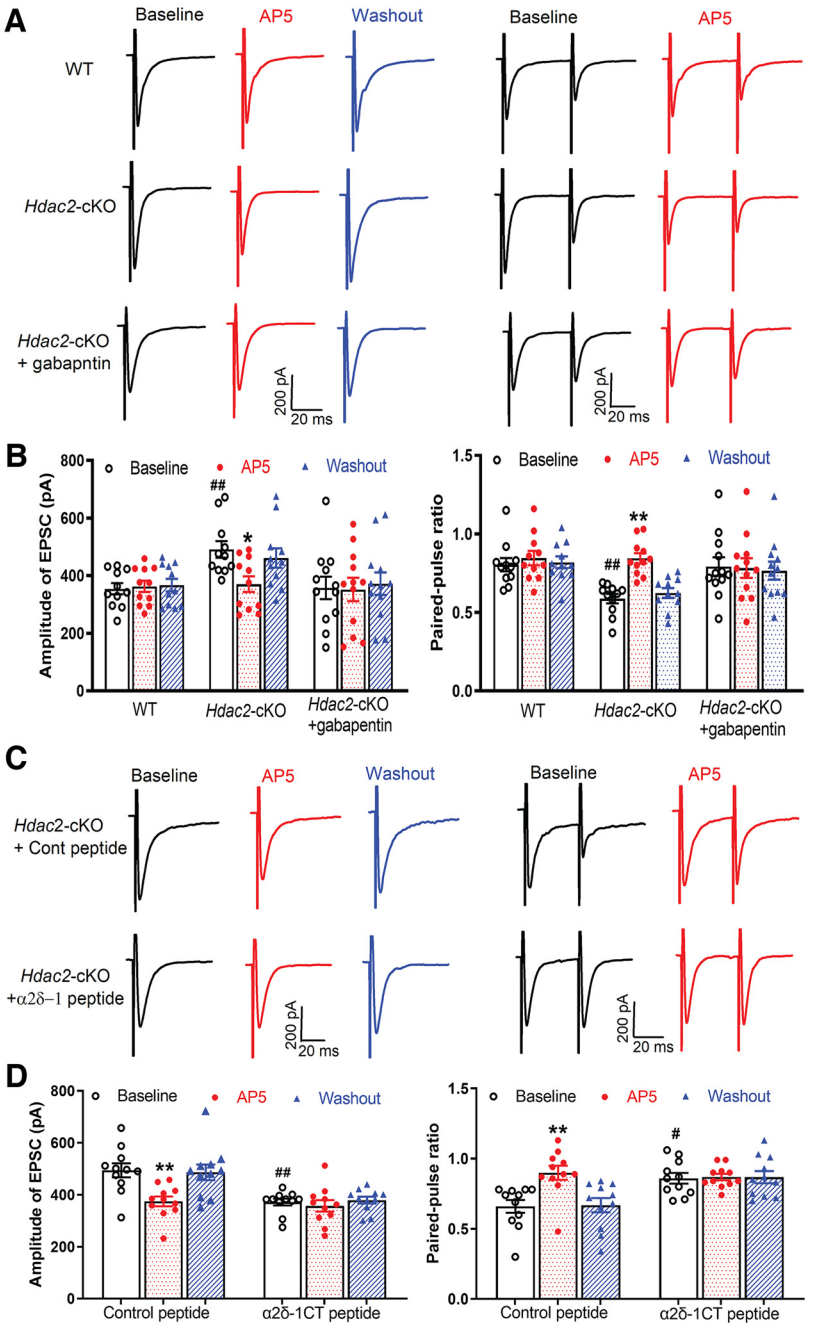

Figure 7. HDAC2 in DRG neurons tonically inhibits α2δ-1–dependent NMDAR activity at primary afferent central terminals. ***A***, ***B***, Representative current traces (***A***) and mean changes (***B***) of EPSCs in spinal lamina II neurons monosynaptically evoked from the dorsal root and EPSCs evoked by a pair of pulses before (Baseline), with (AP5), and after (Washout) bath application of 50 μM AP5. Slice recordings were performed using spinal cords from six WT mice ($n = 11$ neurons), six *Hdac2*-cKO mice ($n = 11$ neurons), and five *Hdac2*-cKO mice pretreated with 100 μM gabapentin ($n = 12$ neurons). Two-way ANOVA (***B***) showed there was a significant main effect for AP5 treatment on the EPSC amplitude ($F_{(2,60)} = 4.199$, $p = 0.0196$) and a significant interaction between the genotype and AP5 treatment ($F_{(2,60)} = 3.283$, $p = 0.0444$). ***C***, ***D***, Original recording traces (***C***) and mean changes (***D***) show the effect of pretreatment with Tat-fused α2δ-1CT peptide or control (Cont) peptide on the amplitude of evoked EPSCs and paired-pulse ratio of evoked EPSCs in spinal lamina II neurons before (Baseline), with (AP5), and after (Washout) bath application of 50 μM AP5. Spinal cord slices were obtained from *Hdac2*-cKO mice and pretreated with 1 μM α2δ-1CT peptide or 1 μM control peptide ($n = 11$ neurons from 5 mice per group). Two-way ANOVA (***D***) showed there was a significant main effect for AP5 treatment on the EPSC amplitude ($F_{(2,60)} = 6.395$, $p = 0.003$) and a significant interaction between the genotype and AP5 treatment ($F_{(2,60)} = 3.405$, $p = 0.0397$); $^{*}p < 0.05$, $^{**}p < 0.01$ versus respective baseline, $^{\#}p < 0.05$, $^{\#\#}p < 0.01$ versus the baseline value in the WT or control peptide group; two-way ANOVA followed by Tukey's *post hoc* test. Data are expressed as means ± SEM.

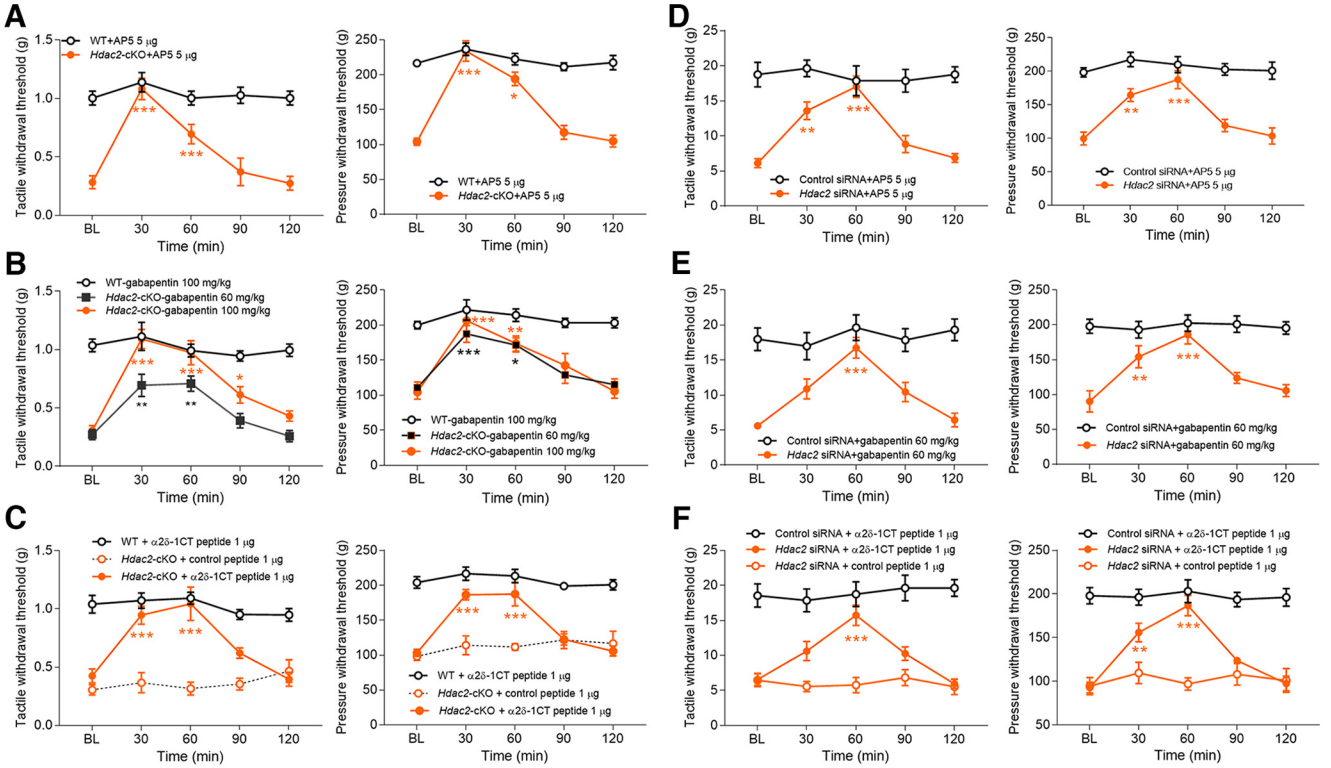

Figure 8. HDAC2 deficiency-induced pain hypersensitivity is maintained by $\alpha2\delta$-1–bound NMDARs at the spinal cord level. ***A–C***, Time course of the effect of AP5 [5 μg, intrathecal (i.t.); ***A***], gabapentin (60 mg/kg or 100 mg/kg, i.p.; ***B***), and $\alpha2\delta$-1CT peptide (1 μg, i.t.; ***C***) on withdrawal thresholds tested with von Frey filaments or a pressure stimulus in *Hdac2*-cKO and WT mice. Two-way ANOVA showed a significant interaction between the genotype and treatment time (***A***; $F_{(4,50)} = 7.765$, $p < 0.001$ for tactile threshold; $F_{(4,50)} = 16.58$, $p < 0.001$ for pressure threshold), (***B***; $F_{(8,95)} = 5.076$, $p < 0.001$ for tactile threshold; $F_{(8,75)} = 2.879$, $p < 0.001$ for pressure threshold), (***C***; $F_{(8,75)} = 5.932$, $p < 0.001$ for tactile threshold; $F_{(8,75)} = 5.346$, $p < 0.001$ for pressure threshold); $^*p < 0.05$, $^{**}p < 0.01$, $^{***}p < 0.001$, compared with baseline (BL), two-way ANOVA with Tukey's *post hoc* test, $n = 8$ mice per group for *Hdac2*-cKO + gabapentin; $n = 6$ mice per group for other groups. ***D–F***, Time course of the effect of AP5 (5 μg, i.t.; ***D***), gabapentin (60 mg/kg, i.p.; ***E***), and $\alpha2\delta$-1CT peptide (1 μg, i.t.; ***F***) on withdrawal thresholds tested with von Frey filaments or a pressure stimulus in *Hdac2*-specific siRNA- or control siRNA-treated rats. Two-way ANOVA showed a significant interaction between the siRNA treatment and drug treatment time (***D***; $F_{(4,55)} = 6.373$, $p = 0.0003$ for tactile threshold; $F_{(4,55)} = 4.599$, $p = 0.0028$ for pressure threshold), (***E***; $F_{(4,55)} = 4.339$, $p = 0.004$ for tactile threshold; $F_{(4,55)} = 4.865$, $p = 0.002$ for pressure threshold), (***F***; $F_{(8,85)} = 3.825$, $p = 0.0007$ for tactile threshold; $F_{(8,85)} = 5.172$, $p < 0.001$ for pressure threshold); $^*p < 0.05$, $^{**}p < 0.01$, $^{***}p < 0.001$, compared with BL, two-way ANOVA with Tukey's *post hoc* test; $n = 6$ rats in the control siRNA group; $n = 7$ rats in the *Hdac2*-siRNA group. Data are expressed as means ± SEM.

al., 1996; Fuller-Bicer et al., 2009), for 30 min normalized the increased frequency of mEPSCs in lamina II neurons ($n = 13$ neurons; Fig. 6*A*,*B*). This increased presynaptic NMDAR activity in the spinal cord by HDAC2 deficiency is similar to that in neuropathic pain conditions (Xie et al., 2016; Chen et al., 2018; Chen et al., 2019). Treatment with gabapentin has no effect on spinal NMDAR activity in WT control mice (Chen et al., 2018; Chen et al., 2019; Deng et al., 2019).

$\alpha2\delta$-1 physically interacts with NMDARs via its C terminus, an intrinsically disordered protein region, and a Tat-fused $\alpha2\delta$-1 C terminus peptide ($\alpha2\delta$-1CT peptide) effectively disrupts the $\alpha2\delta$-1–NMDAR interaction (Chen et al., 2018). Pretreatment of spinal cord slices from *Hdac2*-cKO mice with 1 μM $\alpha2\delta$-1CT peptide, but not 1 μM Tat-fused control peptide, for 30 min normalized the increased frequency of mEPSCs in *Hdac2*-cKO mice ($n = 13$ neurons in control peptide group, $n = 12$ neurons in $\alpha2\delta$-1CT peptide group; Fig. 6*C*,*D*). These results suggest a critical role of $\alpha2\delta$-1–bound NMDARs in HDAC2 deficiency-induced presynaptic NMDAR hyperactivity.

Next, we recorded EPSCs of spinal lamina II neurons monosynaptically evoked by dorsal root stimulation to determine the role of HDAC2 in regulating the activity of NMDARs expressed at primary afferent central terminals. The amplitude of evoked EPSCs of lamina II neurons was significantly larger in *Hdac2*-cKO mice than in WT mice ($p = 0.0080$; $n = 11$ neurons per group; Fig. 7*A*,*B*). Bath application of AP5 rapidly reduced the amplitude of evoked EPSCs of lamina II neurons in *Hdac2*-cKO mice, but not in WT mice (Fig. 7*A*,*B*). Pretreatment of spinal cord slices with gabapentin ($n = 12$ neurons) or $\alpha2\delta$-1CT peptide ($n = 11$ neurons), but not the control peptide ($n = 11$ neurons), also normalized the increased amplitude of evoked monosynaptic EPSCs in *Hdac2*-cKO mice (Fig. 7*C*,*D*).

In addition, the paired-pulse ratio of monosynaptically evoked EPSCs in lamina II neurons was significantly smaller in *Hdac2*-cKO mice than in WT mice ($p = 0.0088$; Fig. 7*A*,*B*). Bath application of AP5 inhibited the first evoked EPSCs more than the second evoked EPSCs, resulting in an increase in the paired-pulse ratio in *Hdac2*-cKO mice (Fig. 7*A*,*B*). Treatment of spinal cord slices with gabapentin or $\alpha2\delta$-1CT peptide, but not the control peptide, also normalized the decreased paired-pulse ratio of evoked EPSCs in *Hdac2*-cKO mice (Fig. 7*C*,*D*). Collectively, these findings are consistent with the notion that HDAC2 in DRG neurons normally suppresses the activity of presynaptic NMDARs at primary afferent central terminals by limiting the availability of $\alpha2\delta$-1 proteins.

HDAC2 in DRG neurons constitutively inhibits pain hypersensitivity by suppressing α2δ-1–NMDAR activity

The important roles of $\alpha2\delta$-1 and NMDARs at the spinal cord level in neuropathic pain are well documented (Zhou et al., 2012;

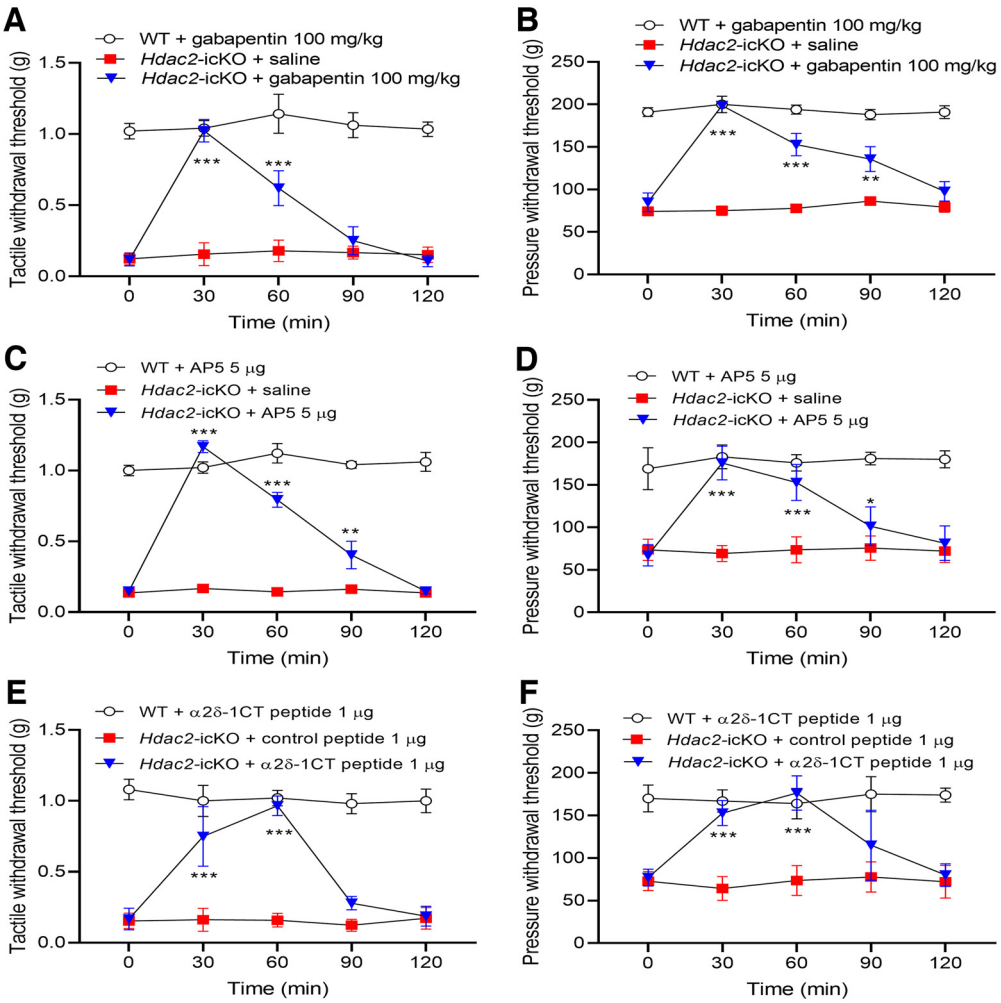

Figure 9. $\alpha2\delta$-1–bound NMDARs at the spinal cord level maintain pain hypersensitivity in *Hdac2*-icKO mice. ***A***, ***B***, Time course of the effect of gabapentin (100 mg/kg, i.p.) on withdrawal thresholds tested with von Frey filaments (***A***) and a pressure stimulus (***B***) in *Hdac2*-icKO or WT mice. ***C***, ***D***, Time course of the effect of AP5 (5 μg, i.t.) on withdrawal thresholds tested with von Frey filaments (***C***) and a pressure stimulus (***D***) in *Hdac2*-icKO or WT mice. ***E***, ***F***, Time course of the effect of $\alpha2\delta$-1CT peptide (1 μg, i.t.) on withdrawal thresholds tested with von Frey filaments (***E***) and a pressure stimulus (***F***) in *Hdac2*-icKO or WT mice. Two-way ANOVA showed a significant interaction between the genotype and drug treatment time ($F_{(8,80)} = 56.94$, $p < 0.0001$ in ***A***; $F_{(8,80)} = 9.475$, $p < 0.0001$ in ***B***; $F_{(8,80)} = 34.94$, $p < 0.0001$ in ***C***; $F_{(8,80)} = 18.33$, $p < 0.0001$ in ***D***; $F_{(8,80)} = 38.85$, $p < 0.0001$ in ***E***; $F_{(8,80)} = 13.5$, $p < 0.0001$ in ***F***); *$p < 0.05$, **$p < 0.01$, ***$p < 0.001$, compared with baseline (time 0), two-way ANOVA with Tukey's *post hoc* test; $n = 7$ *Hdac2*-icKO mice; $n = 5$ WT mice. Data are expressed as means ± SEM.

Chen et al., 2018; Chen et al., 2019). We sought to determine whether HDAC2 in DRG neurons controls pain hypersensitivity via $\alpha2\delta$-1–dependent NMDAR activity. In *Hdac2*-cKO mice, we first tested the effect of intrathecal injection of 5 μg AP5, a specific NMDAR antagonist, on tactile and pressure withdrawal thresholds tested with von Frey filaments and a pressure stimulus. AP5 completely reversed the pain hypersensitivity in *Hdac2*-cKO mice ($n = 6$ mice per group; Fig. 8*A*). Similarly, intraperitoneal injection of 60 mg/kg or 100 mg/kg gabapentin rapidly increased the tactile and pressure withdrawal thresholds that had been reduced in *Hdac2*-cKO mice ($n = 6$ mice for WT; $n = 8$ mice for *Hdac2*-cKO; Fig. 8*B*). Furthermore, intrathecal administration of 1 μg $\alpha2\delta$-1CT peptide, but not 1 μg Tat-fused control peptide, completely reversed the pain hypersensitivity in *Hdac2*-cKO mice ($n = 6$ mice per group; Fig. 8*C*). However, treatment with gabapentin or $\alpha2\delta$-1CT peptide had no effect on the tactile and pressure withdrawal thresholds in WT mice.

In rats intrathecally treated with *Hdac2*-specific siRNA, similar treatment with AP5, gabapentin, or $\alpha2\delta$-1CT peptide normalized the already reduced tactile and pressure withdrawal thresholds ($n = 6$ rats per group for control siRNA; $n = 7$ rats per group for *Hdac2*-specific siRNA; Fig. 8*D–F*). In addition, we assessed and confirmed the same reversal effects of AP5, gabapentin, and $\alpha2\delta$-1CT peptide on the pain hypersensitivity present in tamoxifen-induced *Hdac2*-icKO mice ($n = 5$ WT mice; $n = 7$ *Hdac2*-icKO mice; Fig. 9*A–F*). Together, these data indicate that HDAC2 constitutively represses pain hypersensitivity by limiting $\alpha2\delta$-1–dependent NMDAR activity at the spinal cord level.

Constitutive HDAC2 in DRG neurons restrains pain hypersensitivity mainly via limiting α2δ-1 expression

To investigate other gene targets constitutively regulated by HDAC2 in DRG neurons, we performed RNA-sequencing analysis using L5 and L6 DRGs from *Hdac2*-cKO and WT mice. A total of 210 genes showed a significant increase, whereas 455 genes showed a significant decrease, in *Hdac2*-cKO mice compared with WT mice (Fig. 10*A*,*B*; Extended Data Figs. 10-1, 10-2). These differentially regulated genes were then used for GO analysis. The 210 genes upregulated in *Hdac2*-cKO are enriched in several biological processes, including ion transport, regulation of secretion, T cell activity, intracellular signal transduction,

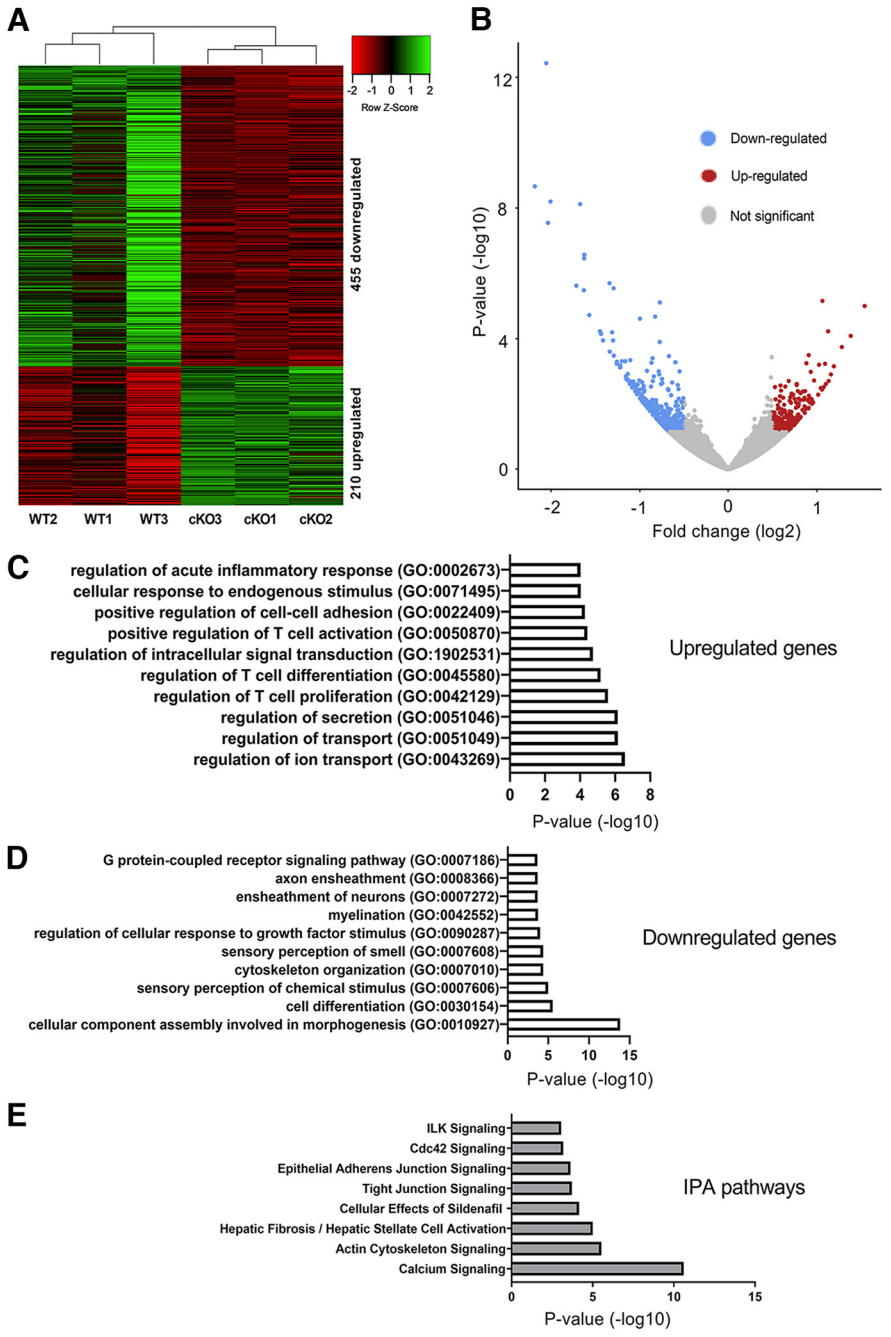

Figure 10. Transcriptome analysis of DRG tissues from WT and *Hdac2*-cKO mice. ***A***, Heat map data show that ablating *Hdac2* in DRG neurons significantly downregulated 455 and upregulated 210 genes ($p < 0.05$) in the DRG. RNA-sequencing data were obtained from three *Hdac2*-cKO (cKO1, cKO2, and cKO3) and three WT (WT1, WT2, and WT3) mice. ***B***, Volcano plot shows differentially expressed genes in the DRG induced by ablating *Hdac2* in DRG neurons. ***C***, ***D***, GO analysis shows the enrichment pathways of upregulated genes (***C***) and downregulated genes (***D***). ***E***, Ingenuity Pathway Analysis (IPA) shows the top eight pathways in which differentially expressed genes are enriched (Extendend Data Figs. 10-1, 10-2, 10-3).

and inflammatory responses (Fig. 10*C*; Extended Data Fig. 10-2). The 455 downregulated genes are enriched in other biological processes, including cellular morphogenesis, cell differentiation, cytoskeletal organization, myelination, and G-protein-coupled receptor signaling pathway (Fig. 10*D*; Extended Data Fig. 10-3). Ingenuity Pathway Analysis indicated that genes with differential expression caused by ablating *Hdac2* in DRG neurons are mainly involved in calcium signaling, actin cytoskeleton signaling, tight junction signaling, and Cdc42 signaling (Fig. 10*E*; Extended Data Fig. 10-3).

Notably, RNA-sequencing data showed that the mRNA level of *Cacna2d1* in the DRG was significantly increased in *Hdac2*-cKO mice compared with WT mice (Extended Data Figs. 10-1, 10-2). We also manually curated a list of differentially regulated genes potentially relevant to nociceptive transduction and transmission. Except for significant changes in a few putative nociceptive genes (e.g., *Il1b* and *P2ry1*), the mRNA levels of pronociceptive genes in the DRG implicated in neuropathic pain, including *Csf1*, *Grm5*, *Scn9a*, *Scn10a*, *Tnf*, and *Tlr4*, did not differ significantly between WT mice and *Hdac2*-cKO mice (Extended Data Figs. 10-1, 10-2). In addition, the mRNA levels of many antinociceptive gene targets, such as potassium channels (e.g., *Kcna4*, *Kcnd2*, and *Kcnq2*), *Oprm1*, *Oprd1*, and *Cnr1*, in the DRG were similar between *Hdac2*-cKO mice and WT mice (Extended Data Figs. 10-1, 10-2).

Finally, we used *Cacna2d1* KO mice to determine to what extent HDAC2 deficiency causes pain hypersensitivity via $\alpha2\delta$-1. We injected intrathecally *Hdac2*-specific siRNA via lumbar puncture in *Cacna2d1* KO mice and WT mice and measured their withdrawal tactile and pressure withdrawal thresholds. Treatment with *Hdac2*-specific siRNA for 5 d in WT mice led to a gradual and profound reduction in the withdrawal thresholds ($p < 0.0001$, $F_{(5,126)} = 15.50$ for tactile threshold; $p < 0.0001$, $F_{(5,126)} = 6.42$ for pressure threshold; Fig. 11*A–C*). By contrast, the reduction in the tactile withdrawal threshold induced by treatment with *Hdac2*-specific siRNA was largely blunted in *Cacna2d1* KO mice ($p = 0.0001$, $F_{(2,261)} = 30.19$; Fig. 11*A*). Furthermore, treatment with *Hdac2*-specific siRNA failed to reduce the pressure withdrawal threshold in *Cacna2d1* KO mice (Fig. 11*B*). These findings suggest that constitutive HDAC2 represses pain hypersensitivity primarily by inhibiting $\alpha2\delta$-1 expression at the spinal cord level.

Discussion

Our study provides substantial new evidence that HDAC2 in primary sensory neurons, via dynamic regulation of histone acetylation status at the *Cacna2d1* promoter, plays a central role in synaptic plasticity associated with neuropathic pain (Fig. 11*D*). Excess $\alpha2\delta$-1 proteins produced by injured DRG neurons mainly amplify nociceptive input by recruiting presynaptic NMDARs at primary afferent central terminals (Chen et al., 2018; Chen et al., 2019; Zhang et al., 2021; Zhou et al., 2021). Thus, sustained upregulation of $\alpha2\delta$-1 in primary sensory neurons plays a key role in the development and maintenance of

neuropathic pain. In this study, our promoter occupancy analysis revealed that nerve injury diminished HDAC2 enrichment at the *Cacna2d1* promoter in the DRG. Importantly, the decrease in HDAC2 binding was accompanied by increased histone H3 and H4 acetylation, particularly H3K9ac and H4K5ac levels, at the *Cacna2d1* promoter. Our findings support the idea that diminished HDAC2 occupancy at the *Cacna2d1* promoter alters the chromatin architecture to promote *Cacna2d1* transcription in DRG neurons after nerve injury. Our discovery of the crucial role of HDAC2 in regulating $\alpha2\delta$-1 expression was unexpected, because nerve injury increases the HDAC2 level in bulk DRG tissues (Laumet et al., 2015). However, global changes in HDAC2 levels in whole DRG tissues cannot predict the abundance of HDAC2 locally at the gene promoter. This critical difference reiterates the importance of determining the binding site occupancy at individual gene promoters to appropriately identify the function of HDAC subtypes in regulating specific gene transcription and chronic pain. Our findings pinpoint that HDAC2 dissociation at the *Cacna2d1* promoter in the DRG constitutes a unique epigenetic mechanism that controls the development of chronic neuropathic pain. It remains unclear how nerve injury diminishes HDAC2 occupancy at the *Cacna2d1* promoter in the DRG. HDAC2 may interact with transcription factors and corepressors, such as SP3, FOXO3a, and coREST (Guan et al., 2009; Formisano et al., 2015; Peng et al., 2015; Yamakawa et al., 2017). Further research is required to define how various transcription factors and corepressors control HDAC2 binding at the *Cacna2d1* promoter in DRG neurons. Until the exact mechanism underlying nerve-injury-induced diminishment of HDAC2 binding at the *Cacna2d1* promoter is known, it is difficult to restore HDAC2 enrichment at the *Cacna2d1* promoter in the injured DRG.

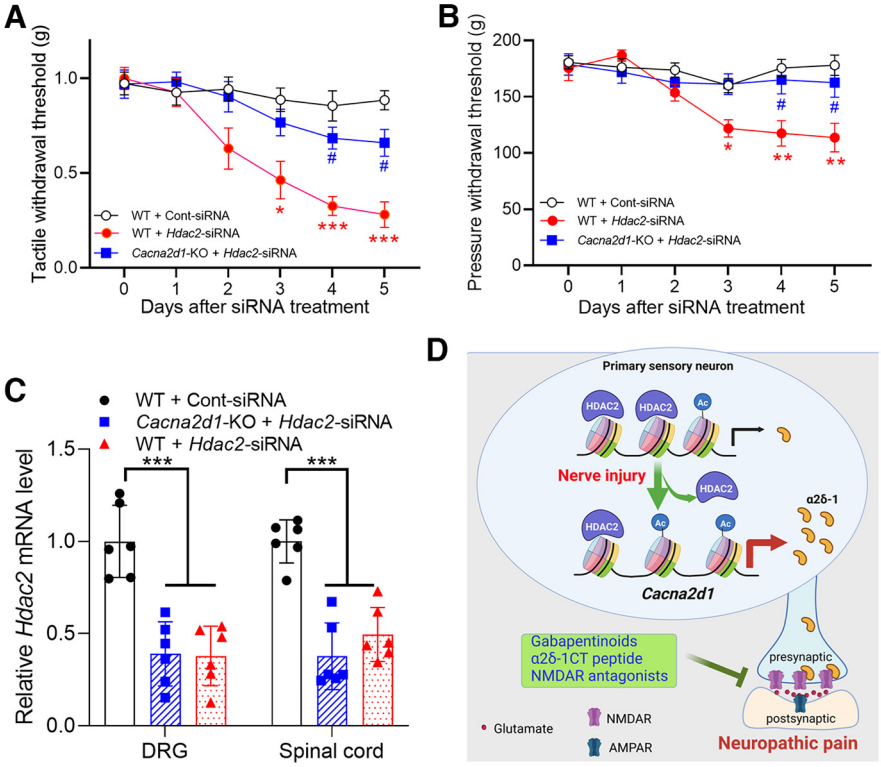

Figure 11. HDAC2 deficiency-induced pain hypersensitivity is blunted in *Cacna2d1* KO mice. ***A***, ***B***, Time course of changes in the withdrawal thresholds tested with von Frey filaments (***A***) and a pressure stimulus (***B***) in WT mice treated intrathecally with control siRNA or *Hdac2*-specific siRNA and in *Cacna2d1* KO mice treated intrathecally with *Hdac2*-specific siRNA. Two-way ANOVA showed a significant interaction between the genotype and siRNA treatment time ($F_{(10,126)} = 3.698$, $p = 0.0002$ in ***A***; $F_{(10,126)} = 3.107$, $p = 0.0014$ in ***B***); $^{*}p < 0.05$, $^{**}p < 0.01$, $^{***}p < 0.001$ versus respective baseline (day 0); $^{\#}p < 0.05$ versus WT mice treated with *Hdac2*-specific siRNA; two-way ANOVA with Tukey's *post hoc* test, $n = 8$ mice per group. ***C***, The *Hdac2* mRNA level in the DRG and spinal cord of *Cacna2d1* KO and WT mice treated with control siRNA or *Hdac2*-specific siRNA; $^{***}p < 0.001$, one-way ANOVA with Dunnett's *post hoc* test, $n = 6$ mice per group. Data are expressed as means ± SEM. ***D***, Schematic illustrates the epigenetic control of $\alpha2\delta$-1 expression and synaptic NMDAR activity by HDAC2 in primary sensory neurons and their central terminals.

Our study reveals that HDAC2 in DRG neurons constitutively controls mechanical pain hypersensitivity. We found that *Hdac2* knockdown at the spinal cord level or *Hdac2* conditional KO in DRG neurons caused a neuropathic pain-like phenotype. Importantly, this phenotype occurred concomitantly with an increase in histone acetylation at the *Cacna2d1* promoter and in $\alpha2\delta$-1 expression. Overexpression of full-length $\alpha2\delta$-1, but not $\alpha2\delta$-1 with C terminus mutations, at the spinal cord level causes a neuropathic pain-like phenotype (Chen et al., 2018; Li et al., 2021). Because HDAC2 is highly enriched at the *Cacna2d1* promoter in the normal DRG, it can constitutively repress *Cacna2d1* transcription via inhibiting histone acetylation at its promoter. Intriguingly, HDAC2 deficiency increased mechanical hypersensitivity, but not cutaneous heat sensitivity. It is unclear why HDAC2 knockdown or cKO increased mechanical, but not heat, sensitivity. Consistent with this phenotype, most patients with neuropathic pain experience mechanical, but not heat, hypersensitivity (Baron and Saguer, 1993; Campbell and Meyer, 2006; Vollert et al., 2017). It is possible that the discrepancy in pain phenotypes caused by nerve injury and HDAC2 knockdown results from $\alpha2\delta$-1 upregulation in different types of DRG neurons. Traumatic nerve injury likely damages both mechano- and heat-sensitive primary afferents to increase $\alpha2\delta$-1 expression in all DRG neurons (Newton et al., 2001; Zhang et al., 2021), whereas $\alpha2\delta$-1 expression controlled by constitutive HDAC2 may be predominantly expressed in mechanosensitive DRG neurons. This could explain the effect of gabapentinoids on both mechano- and heat-hypersensitivity associated with neuropathic pain (Chen et al., 2001; Chen et al., 2019). Remarkably, the pain hypersensitivity caused by HDAC2 deficiency was fully reversed by blocking NMDARs with AP5, inhibiting $\alpha2\delta$-1 with gabapentin, and disrupting the $\alpha2\delta$-1–NMDAR interaction with $\alpha2\delta$-1CT peptide, interventions that are also highly effective for reducing neuropathic pain caused by traumatic nerve injury, small-fiber neuropathy, and chemotherapy (Chen et al., 2018; Chen et al., 2019; Zhang et al., 2021). Our study thus implicates an important protective role of HDAC2 in primary sensory neurons in the transition from acute to chronic neuropathic pain by constitutive repression of *Cacna2d1* transcription.

Another salient finding of our study is that HDAC2 in DRG neurons constitutively regulates synaptic NMDAR activity in the spinal dorsal horn via controlling the expression level of $\alpha2\delta$-1. We showed that the activity of presynaptic NMDARs expressed

at primary afferent central terminals is augmented in *Hdac2*-cKO mice, supporting the critical function of HDAC2 in tonically suppressing nociceptive glutamatergic input to dorsal horn neurons. HDAC2 knockdown also potentiates excitatory synaptic transmission in hippocampal neurons (Hanson et al., 2013), suggesting a wide-ranging role of HDAC2 in regulating synaptic plasticity in the nervous system. NMDARs are expressed at primary afferent central terminals in the spinal cord (Liu et al., 1994); however, these presynaptic NMDARs remain functionally inactive under normal conditions and become active in painful conditions (Chen et al., 2018; Chen et al., 2019; Deng et al., 2019; Huang et al., 2020). We have shown that synaptic expression of NMDARs at primary afferent central terminals requires $\alpha2\delta$-1 proteins (Chen et al., 2018; Zhang et al., 2021; Zhou et al., 2021; Huang et al., 2022). Increased expression of $\alpha2\delta$-1 interacts with NMDARs via its C terminus to augment their synaptic trafficking, causing tonic activation of synaptic NMDARs at the spinal cord level in neuropathic pain (Chen et al., 2018). Our findings suggest that NMDARs that are present at primary afferent central terminals are latent because of limited availability of $\alpha2\delta$-1 and its interaction with NMDARs. This notion is supported by our findings that inhibiting $\alpha2\delta$-1 with gabapentin or disrupting the $\alpha2\delta$-1–NMDAR complex reversed the potentiated NMDAR activity in the spinal dorsal horn caused by ablating HDAC2 in DRG neurons. Thus, HDAC2 in DRG neurons normally restrains nociceptive input to the spinal cord by inhibiting $\alpha2\delta$-1 expression and ensuing NMDAR activity at primary afferent central terminals.

RNA-sequencing data from *Hdac2*-cKO mice confirmed that *Cacna2d1* is the key nociceptive gene regulated by HDAC2 in the DRG. We cannot, however, exclude the possibility that other gene targets are involved in HDAC2 deficiency-induced pain hypersensitivity. By inspecting the list of differentially regulated genes from RNA-sequencing data, we noted that some gene targets implicated in promoting pain, such as interleukin-1β (*Il1b*) and purinergic receptor P2Y1 (*P2ry1*), are also upregulated in the DRG of *Hdac2*-cKO mice. It is possible that the transcription of *Il1b* and *P2ry1* is also controlled directly by HDAC2. Interleukin-1β and purinergic receptor P2Y1 may promote nociception by increasing the excitability of DRG neurons (Nakamura and Strittmatter, 1996; Stemkowski and Smith, 2012). However, their roles in the development of chronic pain are uncertain because nerve injury reduces the expression level of *P2ry1* in the DRG (Laumet et al., 2015) and because intrathecal injection of interleukin-1β attenuates inflammatory pain (Souter et al., 2000). Importantly, we showed in this study that HDAC2 knockdown with siRNA had little effect in inducing pain hypersensitivity in *Cacna2d1* KO mice. This finding further supports our interpretation that HDAC2 in DRG neurons constitutively restrains pain hypersensitivity predominantly via regulating $\alpha2\delta$-1 expression.

HDAC subtypes have diverse functions in the nervous system (Broide et al., 2007; Guan et al., 2009). Previous studies, largely using nonspecific HDAC inhibitors, provided only conflicting results about the functions of individual HDAC subtypes in pain regulation. In this regard, some HDAC inhibitors, including suberoylanilide hydroxamic acid, LG325, and MS-275, slightly reduce nerve injury-induced neuropathic pain (Denk et al., 2013; Laumet et al., 2015; Sanna et al., 2017), whereas other HDAC inhibitors, such as JNJ-26481585, cause pain hypersensitivity in normal animals (Capasso et al., 2015). Interestingly, systemic treatment with JNJ-26481585 increases $\alpha2\delta$-1 expression in the spinal cord, and gabapentin effectively reverses mechanical pain hypersensitivity caused by JNJ-26481585 (Capasso et al., 2015). Thus, by extension, our findings suggest that JNJ-26481585 may cause pain hypersensitivity mainly via inhibiting HDAC2 activity in the DRG and spinal cord.

In summary, we discovered that HDAC2 in primary sensory neurons is a pivotal epigenetic regulator of synaptic plasticity and nociception. The physiological role of HDAC2 is to function as a key transcriptional repressor to restrain pain hypersensitivity by constitutively inhibiting $\alpha2\delta$-1 expression in primary sensory neurons and ensuing presynaptic NMDAR activity in the spinal dorsal horn. Correspondingly, the loss of HDAC2 binding at the *Cacna2d1* promoter could facilitate the transition from acute to chronic pain after nerve injury by potentiating $\alpha2\delta$-1 expression and $\alpha2\delta$-1–dependent synaptic NMDAR activity. This information not only advances our mechanistic understanding of epigenetic control of synaptic plasticity in neuropathic pain but also can guide the treatment of adverse effects of HDAC inhibitors that are clinically used for treating several types of cancers. Pain is likely associated with HDAC inhibitors that impair HDAC2 activity, and $\alpha2\delta$-1–bound NMDARs can be targeted for treating this painful condition. Furthermore, because of long-lasting $\alpha2\delta$-1 upregulation in neuropathic pain conditions, gabapentinoids relieve pain symptoms only temporarily. Our study suggests that restoring the normal function of HDAC2 and/or reducing histone acetylation at the *Cacna2d1* promoter in primary sensory neurons may lead to long-lasting relief of neuropathic pain.

References

Baron R, Saguer M (1993) Postherpetic neuralgia. Are C-nociceptors involved in signalling and maintenance of tactile allodynia? Brain 116:1477–1496.

Broide RS, Redwine JM, Aftahi N, Young W, Bloom FE, Winrow CJ (2007) Distribution of histone deacetylases 1-11 in the rat brain. J Mol Neurosci 31:47–58.

Campbell JN, Meyer RA (2006) Mechanisms of neuropathic pain. Neuron 52:77–92.

Capasso KE, Manners MT, Quershi RA, Tian Y, Gao R, Hu H, Barrett JE, Sacan A, Ajit SK (2015) Effect of histone deacetylase inhibitor JNJ-26481585 in pain. J Mol Neurosci 55:570–578.

Chaplan SR, Bach FW, Pogrel JW, Chung JM, Yaksh TL (1994) Quantitative assessment of tactile allodynia in the rat paw. J Neurosci Methods 53:55–63.

Chen J, Li L, Chen SR, Chen H, Xie JD, Sirrieh RE, MacLean DM, Zhang Y, Zhou MH, Jayaraman V, Pan HL (2018) The $\alpha2\delta$-1-NMDA receptor complex is critically involved in neuropathic pain development and gabapentin therapeutic actions. Cell Rep 22:2307–2321.

Chen SR, Pan HL (2001) Spinal endogenous acetylcholine contributes to the analgesic effect of systemic morphine in rats. Anesthesiology 95:525–530.

Chen SR, Xu Z, Pan HL (2001) Stereospecific effect of pregabalin on ectopic afferent discharges and neuropathic pain induced by sciatic nerve ligation in rats. Anesthesiology 95:1473–1479.

Chen SR, Hu YM, Chen H, Pan HL (2014a) Calcineurin inhibitor induces pain hypersensitivity by potentiating pre- and postsynaptic NMDA receptor activity in spinal cords. J Physiol 592:215–227.

Chen SR, Zhou HY, Byun HS, Chen H, Pan HL (2014b) Casein kinase II regulates N-methyl-D-aspartate receptor activity in spinal cords and pain hypersensitivity induced by nerve injury. J Pharmacol Exp Ther 350:301–312.

Chen Y, Chen SR, Chen H, Zhang J, Pan HL (2019) Increased $\alpha2\delta$-1-NMDA receptor coupling potentiates glutamatergic input to spinal dorsal horn neurons in chemotherapy-induced neuropathic pain. J Neurochem 148:252–274.

da Silva S, Hasegawa H, Scott A, Zhou X, Wagner AK, Han BX, Wang F (2011) Proper formation of whisker barrelettes requires periphery-

derived Smad4-dependent TGF-beta signaling. Proc Natl Acad Sci U S A 108:3395–3400.

Deng M, Chen SR, Chen H, Pan HL (2019) $\alpha2\delta$-1-bound N-methyl-D-aspartate receptors mediate morphine-induced hyperalgesia and analgesic tolerance by potentiating glutamatergic input in rodents. Anesthesiology 130:804–819.

Denk F, Huang W, Sidders B, Bithell A, Crow M, Grist J, Sharma S, Ziemek D, Rice AS, Buckley NJ, McMahon SB (2013) HDAC inhibitors attenuate the development of hypersensitivity in models of neuropathic pain. Pain 154:1668–1679.

Formisano L, Guida N, Valsecchi V, Cantile M, Cuomo O, Vinciguerra A, Laudati G, Pignataro G, Sirabella R, Di Renzo G, Annunziato L (2015) Sp3/REST/HDAC1/HDAC2 complex represses and Sp1/HIF-1/p300 complex activates ncx1 gene transcription, in brain ischemia and in ischemic brain preconditioning, by epigenetic mechanism. J Neurosci 35:7332–7348.

Fuller-Bicer GA, Varadi G, Koch SE, Ishii M, Bodi I, Kadeer N, Muth JN, Mikala G, Petrashevskaya NN, Jordan MA, Zhang SP, Qin N, Flores CM, Isaacsohn I, Varadi M, Mori Y, Jones WK, Schwartz A (2009) Targeted disruption of the voltage-dependent calcium channel alpha2/delta-1-subunit. Am J Physiol Heart Circ Physiol 297:H117–124.

Garriga J, Laumet G, Chen SR, Zhang Y, Madzo J, Issa JJ, Pan HL, Jelinek J (2018) Nerve injury-induced chronic pain is associated with persistent DNA methylation reprogramming in dorsal root ganglion. J Neurosci 38:6090–6101.

Gee NS, Brown JP, Dissanayake VU, Offord J, Thurlow R, Woodruff GN (1996) The novel anticonvulsant drug, gabapentin (Neurontin), binds to the alpha2delta subunit of a calcium channel. J Biol Chem 271:5768–5776.

Ghosh K, Zhang GF, Chen H, Chen SR, Pan HL (2022) Cannabinoid CB2 receptors are upregulated via bivalent histone modifications and control primary afferent input to the spinal cord in neuropathic pain. J Biol Chem 298:101999.

Guan JS, Haggarty SJ, Giacometti E, Dannenberg JH, Joseph N, Gao J, Nieland TJ, Zhou Y, Wang X, Mazitschek R, Bradner JE, DePinho RA, Jaenisch R, Tsai LH (2009) HDAC2 negatively regulates memory formation and synaptic plasticity. Nature 459:55–60.

Hanson JE, Deng L, Hackos DH, Lo SC, Lauffer BE, Steiner P, Zhou Q (2013) Histone deacetylase 2 cell autonomously suppresses excitatory and enhances inhibitory synaptic function in CA1 pyramidal neurons. J Neurosci 33:5924–5929.

Hervera A, Zhou L, Palmisano I, McLachlan E, Kong G, Hutson TH, Danzi MC, Lemmon VP, Bixby JL, Matamoros-Angles A, Forsberg K, De Virgiliis F, Matheos DP, Kwapis J, Wood MA, Puttagunta R, Del Río JA, Di Giovanni S (2019) PP4-dependent HDAC3 dephosphorylation discriminates between axonal regeneration and regenerative failure. EMBO J 38:e101032.

Huang Y, Chen SR, Chen H, Luo Y, Pan HL (2020) Calcineurin inhibition causes $\alpha2\delta$-1-mediated tonic activation of synaptic NMDA receptors and pain hypersensitivity. J Neurosci 40:3707–3719.

Huang Y, Chen SR, Chen H, Zhou JJ, Jin D, Pan HL (2022) Theta-burst stimulation of primary afferents drives long-term potentiation in the spinal cord and persistent pain via $\alpha2\delta$-1-bound NMDA receptors. J Neurosci 42:513–527.

Jiang Y, Langley B, Lubin FD, Renthal W, Wood MA, Yasui DH, Kumar A, Nestler EJ, Akbarian S, Beckel-Mitchener AC (2008) Epigenetics in the nervous system. J Neurosci 28:11753–11759.

Jin D, Chen H, Huang Y, Chen SR, Pan HL (2022) δ-Opioid receptors in primary sensory neurons tonically restrain nociceptive input in chronic pain but do not enhance morphine analgesic tolerance. Neuropharmacology 217:109202.

Kim D, Langmead B, Salzberg SL (2015) HISAT: a fast spliced aligner with low memory requirements. Nat Methods 12:357–360.

Kim SH, Chung JM (1992) An experimental model for peripheral neuropathy produced by segmental spinal nerve ligation in the rat. Pain 50:355–363.

Krämer A, Green J, Pollard J Jr, Tugendreich S (2014) Causal analysis approaches in Ingenuity Pathway Analysis. Bioinformatics 30:523–530.

Lau J, Minett MS, Zhao J, Dennehy U, Wang F, Wood JN, Bogdanov YD (2011) Temporal control of gene deletion in sensory ganglia using a tamoxifen-inducible Advillin-Cre-ERT2 recombinase mouse. Mol Pain 7:100.

Laumet G, Garriga J, Chen SR, Zhang Y, Li DP, Smith TM, Dong Y, Jelinek J, Cesaroni M, Issa JP, Pan HL (2015) G9a is essential for epigenetic silencing of K(+) channel genes in acute-to-chronic pain transition. Nat Neurosci 18:1746–1755.

Li DP, Chen SR, Pan YZ, Levey AI, Pan HL (2002) Role of presynaptic muscarinic and GABA(B) receptors in spinal glutamate release and cholinergic analgesia in rats. J Physiol 543:807–818.

Li H, Handsaker B, Wysoker A, Fennell T, Ruan J, Homer N, Marth G, Abecasis G, Durbin R (2009) The Sequence Alignment/Map format and SAMtools. Bioinformatics 25:2078–2079.

Li L, Chen SR, Chen H, Wen L, Hittelman WN, Xie JD, Pan HL (2016) Chloride homeostasis critically regulates synaptic NMDA receptor activity in neuropathic pain. Cell Rep 15:1376–1383.

Li L, Chen SR, Zhou MH, Wang L, Li DP, Chen H, Lee G, Jayaraman V, Pan HL (2021) $\alpha2\delta$-1 switches the phenotype of synaptic AMPA receptors by physically disrupting heteromeric subunit assembly. Cell Rep 36:109396.

Li JQ, Chen SR, Chen H, Cai YQ, Pan HL (2010) Regulation of increased glutamatergic input to spinal dorsal horn neurons by mGluR5 in diabetic neuropathic pain. J Neurochem 112:162–172.

Liao Y, Smyth GK, Shi W (2014) featureCounts: an efficient general purpose program for assigning sequence reads to genomic features. Bioinformatics 30:923–930.

Liu H, Wang H, Sheng M, Jan LY, Jan YN, Basbaum AI (1994) Evidence for presynaptic N-methyl-D-aspartate autoreceptors in the spinal cord dorsal horn. Proc Natl Acad Sci U S A 91:8383–8387.

Love MI, Huber W, Anders S (2014) Moderated estimation of fold change and dispersion for RNA-seq data with DESeq2. Genome Biol 15:550.

Luo Y, Zhang J, Chen L, Chen SR, Chen H, Zhang G, Pan HL (2020) Histone methyltransferase G9a diminishes expression of cannabinoid CB(1) receptors in primary sensory neurons in neuropathic pain. J Biol Chem 295:3553–3562.

Luo ZD, Chaplan SR, Higuera ES, Sorkin LS, Stauderman KA, Williams ME, Yaksh TL (2001) Upregulation of dorsal root ganglion (alpha)2(delta) calcium channel subunit and its correlation with allodynia in spinal nerve-injured rats. J Neurosci 21:1868–1875.

Mi H, Muruganujan A, Ebert D, Huang X, Thomas PD (2019) PANTHER version 14: more genomes, a new PANTHER GO-slim and improvements in enrichment analysis tools. Nucleic Acids Res 47:D419–D426.

Nakamura F, Strittmatter SM (1996) P2Y1 purinergic receptors in sensory neurons: contribution to touch-induced impulse generation. Proc Natl Acad Sci U S A 93:10465–10470.

Newton RA, Bingham S, Case PC, Sanger GJ, Lawson SN (2001) Dorsal root ganglion neurons show increased expression of the calcium channel alpha2delta-1 subunit following partial sciatic nerve injury. Mol Brain Res 95:1–8.

Peng S, Zhao S, Yan F, Cheng J, Huang L, Chen H, Liu Q, Ji X, Yuan Z (2015) HDAC2 selectively regulates FOXO3a-mediated gene transcription during oxidative stress-induced neuronal cell death. J Neurosci 35:1250–1259.

Sanna MD, Guandalini L, Romanelli MN, Galeotti N (2017) The new HDAC1 inhibitor LG325 ameliorates neuropathic pain in a mouse model. Pharmacol Biochem Behav 160:70–75.

Santos SF, Rebelo S, Derkach VA, Safronov BV (2007) Excitatory interneurons dominate sensory processing in the spinal substantia gelatinosa of rat. J Physiol 581:241–254.

Souter AJ, Garry MG, Tanelian DL (2000) Spinal interleukin-1beta reduces inflammatory pain. Pain 86:63–68.

Stemkowski PL, Smith PA (2012) Long-term IL-1β exposure causes subpopulation-dependent alterations in rat dorsal root ganglion neuron excitability. J Neurophysiol 107:1586–1597.

Strahl BD, Allis CD (2000) The language of covalent histone modifications. Nature 403:41–45.

Vollert J, et al. (2017) Stratifying patients with peripheral neuropathic pain based on sensory profiles: algorithm and sample size recommendations. Pain 158:1446–1455.

Wang L, Chen SR, Ma H, Chen H, Hittelman WN, Pan HL (2018) Regulating nociceptive transmission by VGluT2-expressing spinal dorsal horn neurons. J Neurochem 147:526–540.

Wilting RH, Yanover E, Heideman MR, Jacobs H, Horner J, van der Torre J, DePinho RA, Dannenberg JH (2010) Overlapping functions of Hdac1

and Hdac2 in cell cycle regulation and haematopoiesis. Embo J 29:2586–2597.

Woo SH, Ranade S, Weyer AD, Dubin AE, Baba Y, Qiu Z, Petrus M, Miyamoto T, Reddy K, Lumpkin EA, Stucky CL, Patapoutian A (2014) Piezo2 is required for Merkel-cell mechanotransduction. Nature 509:622–626.

Woolf CJ, Salter MW (2000) Neuronal plasticity: increasing the gain in pain. Science 288:1765–1769.

Xie JD, Chen SR, Chen H, Zeng WA, Pan HL (2016) Presynaptic *N*-methyl-D-aspartate (NMDA) receptor activity is increased through protein kinase C in paclitaxel-induced neuropathic pain. J Biol Chem 291:19364–19373.

Xie JD, Chen SR, Chen H, Pan HL (2017) Bortezomib induces neuropathic pain through protein kinase C-mediated activation of presynaptic NMDA receptors in the spinal cord. Neuropharmacology 123:477–487.

Yamakawa H, Cheng J, Penney J, Gao F, Rueda R, Wang J, Yamakawa S, Kritskiy O, Gjoneska E, Tsai LH (2017) The transcription factor Sp3 cooperates with HDAC2 to regulate synaptic function and plasticity in neurons. Cell Rep 20:1319–1334.

Zappia KJ, O'Hara CL, Moehring F, Kwan KY, Stucky CL (2017) Sensory neuron-specific deletion of TRPA1 results in mechanical cutaneous sensory deficits. eNeuro 4:ENEURO.0069-16.2017.

Zhang GF, Chen SR, Jin D, Huang Y, Chen H, Pan HL (2021) Upregulation in primary sensory neurons promotes NMDA receptor-mediated glutamatergic input in resiniferatoxin-induced neuropathy. J Neurosci 41:5963–5978.

Zhang HM, Chen SR, Pan HL (2009) Effects of activation of group III metabotropic glutamate receptors on spinal synaptic transmission in a rat model of neuropathic pain. Neuroscience 158:875–884.

Zhang J, Chen SR, Chen H, Pan HL (2018) RE1-silencing transcription factor controls the acute-to-chronic neuropathic pain transition and Chrm2 receptor gene expression in primary sensory neurons. J Biol Chem 293:19078–19091.

Zhang YH, Chen SR, Laumet G, Chen H, Pan HL (2016) Nerve injury diminishes opioid analgesia through lysine methyltransferase-mediated transcriptional repression of μ-opioid receptors in primary sensory neurons. J Biol Chem 291:8475–8485.

Zhou HY, Chen SR, Chen H, Pan HL (2010) Opioid-induced long-term potentiation in the spinal cord is a presynaptic event. J Neurosci 30:4460–4466.

Zhou HY, Chen SR, Pan HL (2011) Targeting N-methyl-D-aspartate receptors for treatment of neuropathic pain. Expert Rev Clin Pharmacol 4:379–388.

Zhou HY, Chen SR, Byun HS, Chen H, Li L, Han HD, Lopez-Berestein G, Sood AK, Pan HL (2012) N-methyl-D-aspartate receptor- and calpain-mediated proteolytic cleavage of K+-Cl- cotransporter-2 impairs spinal chloride homeostasis in neuropathic pain. J Biol Chem 287:33853–33864.

Zhou MH, Chen SR, Wang L, Huang Y, Deng M, Zhang J, Zhang J, Chen H, Yan J, Pan HL (2021) Protein kinase C-mediated phosphorylation and $\alpha 2\delta$-1 interdependently regulate NMDA receptor trafficking and activity. J Neurosci 41:6415–6429.

Zhou X, Wang L, Hasegawa H, Amin P, Han BX, Kaneko S, He Y, Wang F (2010) Deletion of PIK3C3/Vps34 in sensory neurons causes rapid neurodegeneration by disrupting the endosomal but not the autophagic pathway. Proc Natl Acad Sci U S A 107:9424–9429.